colorants

MDPI

Review

Plant-Mediated Synthesis of NiO Nanoparticles for Textile Dye Degradation in Water: A Review

Itumeleng Seete [1], Dineo A. Bopape [2], Louisah M. Mahlaule-Glory [1], Zikhona Tetana [3] and Nomso C. Hintsho-Mbita [1,*]

[1] Department of Chemistry, University of Limpopo, Sovenga 0727, South Africa
[2] Department of Mathematics, Science and Technology Education (DMSTE), University of Limpopo, Sovenga 0727, South Africa; dineo.bopape@ul.ac.za
[3] Institute for Nanotechnology and Water Sustainability (iNanoWS), College of Science, Engineering and Technology, University of South Africa, Florida 1709, South Africa; tetanzn@unisa.ac.za
* Correspondence: nomso.hintsho-mbita@ul.ac.za

Abstract: Water contamination caused by dyes from increased human activities, in particular usage in the textile sector, has led to high rates of disposal of both natural and synthetic dyes in the water stream, affecting the color and the ability of the light to penetrate through the water system. Several methods have been used for the removal of these organic pollutants. However, due to the complex nature of these dyes, researchers have geared toward advanced oxidation processes (AOPs). This method allows for the degradation of these pollutants into more environmentally friendly pollutants. Green synthesis of known catalysts has been on the rise, in particular nickel oxide (NiO) NPs. This material has been shown to have the ability to degrade several pollutants. However, due to the high recombination rate and large bandgap, their limitation has also been highlighted along with the importance of modification. Thus, it is important to understand the work and progress made on green NiO as a photocatalyst for the degradation of dyes and the latest advancements in the field.

Keywords: dye colorants; NiO NPs; water treatment; green synthesis; photocatalysis

Academic Editor: Radosław Podsiadły

Received: 30 November 2024
Revised: 28 January 2025
Accepted: 4 February 2025
Published: 18 February 2025

Citation: Seete, I.; Bopape, D.A.; Mahlaule-Glory, L.M.; Tetana, Z.; Hintsho-Mbita, N.C. Plant-Mediated Synthesis of NiO Nanoparticles for Textile Dye Degradation in Water: A Review. *Colorants* **2025**, *4*, 7. https://doi.org/10.3390/colorants4010007

1. Introduction

Water contamination is a global problem that researchers have been trying to overcome, as these contaminants are harmful to aquatic life and are carcinogenic [1]. These contaminants are caused by industrial pollution, agricultural runoff, wastewater disposal, mining activities, and oil spills [2]. One of the industrial polluting areas is the textile industry. This industry contributes 8% of all carbon emissions and 20% of all global wastewater [3]. The most commonly used dyes include methylene blue (MB), malachite green (MG), methyl orange (MO), methyl violet (MV), and many more, with some remaining in water even after treatment (Figure 1) [4]. The usage of these dyes has expanded to so many industries. Of the more significant are the textile, food, and medical industries. In the textile industry, the focus is mainly on clothing and colored fabrics. As part of the food industry, these dyes are added to food to enhance the visual appeal and improve flavor [5]. In entertainment, these can be used for makeup and skin care [6–8]. And more importantly, the medical industry uses these dyes largely in biological applications for the staining of tissues to assist with the identification of cells under microscopy and as fluorescent markers [9,10].

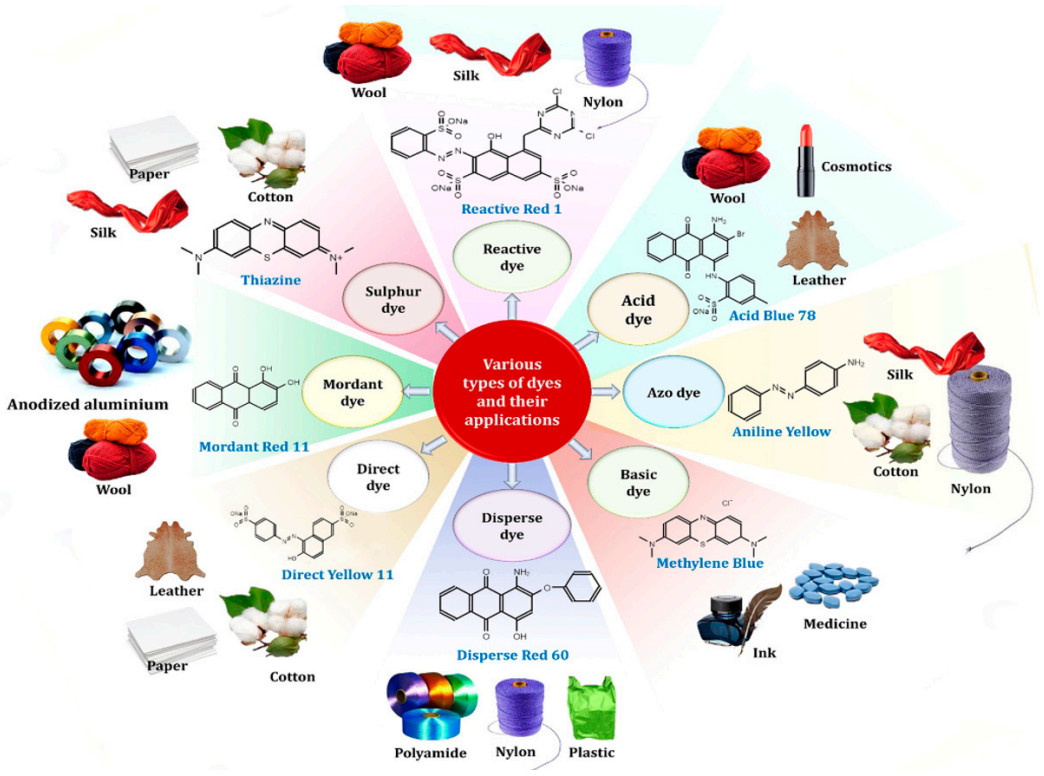

Figure 1. Dyes and their various applications [4]. Open access (OA).

Untreated dyes cause the coloration of water, which negatively affects photosynthesis for aquatic plants [3]. The annual production of synthetic dyes is 7×10^7 tons worldwide, with over 10,000 tons from the textile industry [11–14]. Countries such as China, India, and Bangladesh are some of the biggest contributors of these pollutants and release a combined 3.5 billion tons of textile wastewater annually [4]. There are a lot of factors that affect the removal or degradation of dyes, such as concentration, electron charge, and pH [5,15–18]. Researchers have tried using several methods, such as reverse osmosis, activated sludge, coagulation, electrochemical oxidation, adsorption, and photocatalysis, for the removal of these pollutants [6–8]. Although these methods have been widely used (Table 1), they do suffer from some limitations, and their applicability is dependent upon factors such as cost and time, to mention a few [6]. For example, with activated sludge, micro-organisms are utilized for the treatment of municipal and industrial wastewater. Several steps, such as separation, aeration, and recycling, are followed to ensure that the method is effective [19,20]. This method, on top of requiring several steps, also requires sludge disposal, high operational costs, and is not flexible, as it only targets a limited number of pollutants. Whereas coagulation mainly focuses on the removal of solids using highly charged molecules to destabilize the particles, though effective, a possible formation of sludges might take place [8]. With electro-oxidation, although it is one of the popular AOP methods, it is mainly limited to the degradation of pesticides and microplastics [9].

Recently, researchers have been tilting towards the use of photocatalysis for the degradation of dyes because of its benefits, such as being environmentally friendly and low in cost [21–24]. Photocatalysis involves the use of light at a certain wavelength to degrade water pollutants, such as dyes. In photocatalysis (Figure 2), an electro-hole formation is generated due to the exposure of light to the semiconductor. The photocatalysts are used to absorb light and work as a catalyst for chemical reactions [12,25].

Table 1. Traditional water treatment methods for the removal of textile dyes.

Treatment Methods	Treatment Processes	Function	Advantages	Disadvantages	Refs
Active Sludge	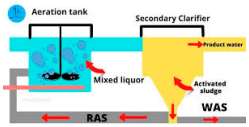	Mainly used in cleaning sewage water. It involves the use of oxygen for treatment.	Need for less space Good quality effluent	High operating cost Sensitive process	[7]
Coagulation	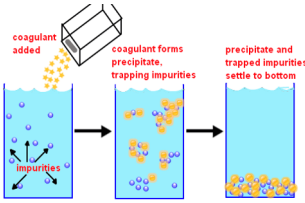	It is a chemical method involving the manipulation of contaminants electrostatic charges in water.	Effective removal of pollutants	Need for additional chemicals. Possible formation of a sludge	[8]
Electrochemical Oxidation	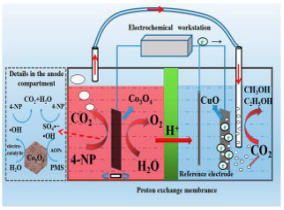	It is a chemical process where electrodes are placed in a container containing water waste to degrade the pollutants partially or fully.	No addition of chemicals required	BDD cells are highly cost-prohibitive.	[9]
Photocatalysis	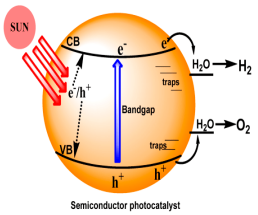	Involves the use of light and a semiconductor to degrade pollutants.	Inexpensive. Low environmental effect	Not visible-light active, meaning they will result in low activity.	[10]
Reverse Osmosis	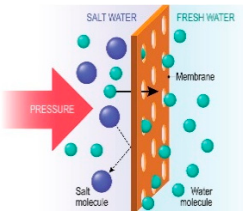	Highly concentrated contaminants are moved through a semi-permeable membrane to a low-concentrated one.	No energy costs. Better tasting. Less odor and pleasing appearance	Cannot remove microorganisms such as viruses and bacteria	[11]

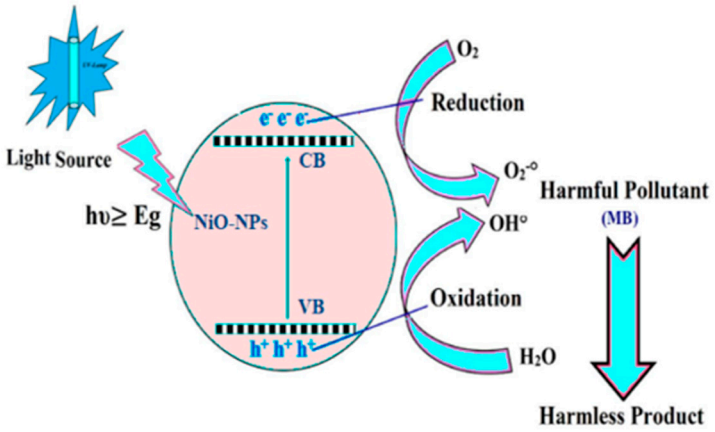

Figure 2. Photocatalysis process of NiO against dyes [12].

Several types of photocatalysts are being used in the photocatalysis process, and these include ZnO, NiO, CuO, ZnS, and SnO_2 [25–27]. They are preferred because of their properties, such as easy penetration of light, high chemical reactivity, stability, sensitivity,

and a large surface area [13,14,28]. NiO differs from other semiconductors like TiO_2 because it possesses p-type semiconductor characteristics [29,30]. As a material, it has a higher mobility charge, which allows for a better electron transfer. Also, as a photocatalyst, it can absorb in the visible region as well, thus increasing its efficiency for degradation [31]. Although it has these admirable properties compared to TiO_2, it still performs better as a composite with TiO_2, as it forms a p-n heterojunction [32,33].

NiO is a p-type semiconductor that is known for its use in various applications [14]. These include environmental, energy, electronic, and medicinal [15–17]. In electronics, they are used as semiconductors, radar-absorbing materials, and electrochromic devices [18–20]. For medicine, NiO NPs mostly function as drug delivery devices, as antibiotics, and in biomedical imaging [21,22]. Ezhilarasi et al. [34] used moringa-mediated NiO to demonstrate the cytotoxic effect of NiO NPs against the human cancer cell HT-25. From their analysis, apoptosis was induced. As a photocatalyst, it has its benefits, such as being affordable and having photostability, and high chemical stability in electro-optical efficiency, which is why it is an efficient photocatalyst [35–37]. Despite the many advantages NiO has, it also possesses limitations, such as a high bandgap energy of 3.6–4.0 eV, a fast recombination rate, and synthesis through the chemical route [38–40]. Thus, researchers have opted to introduce a metal to form a bimetallic structure or form heterostructures in an effort to reduce its band energy [41]. Also, due to the harmful solvents currently being used, researchers have opted for the synthesis of these materials using green materials as reducing agents, such as plants, bacteria, and fungi [42–44]. The usage of plant extracts has been the most preferred due to costs, the availability of the plants, and the ease of usage [45–52]. The use of fungi and bacteria has mostly presented challenges, such as multiple steps that are required to maintain the cell before synthesis and the production of agglomerated and non-uniform particles [53,54]. Hence, plant-mediated synthesis is on the rise [55–59]. Mandal et al. [60] used *Punica granatum* to form ferromagnetic NiO NPs with a fcc cubic structure and nanoparticles with a size of 13–42 nm, and these could be used in the degradation of MO. Prabhu et al. [61] used a *Clitoria ternatea* flower extract to synthesize hexagonally shaped NiO NPs. From their material, they were able to degrade 89% of Fast green dye (FG) and 77% of Rose Bengal (Rb) in the presence of sunlight [61]. Karthik et al. [17] formed cubic NiO from *Andographas paniculata* leaf extracts with a crystallite size of 24 nm and a bandgap of 3.51 eV. They noted that the material could be used for the degradation of Evans Blue dye.

Though several materials had been constructed from the synthesis of NiO materials from plant extracts, it can be noted that various optical, physical, and surface properties were formed [19]. These could be due to the various phytochemicals found in these plants, leading to distinctly different properties and catalytic performances in wastewater against various pollutants [62–64].

Thus, in this review, we explore the properties and green synthetic routes for NiO NPs. The usage of these plant-derived materials as photocatalysts for the degradation of dyes and their modification is also highlighted. Lastly, their use for the degradation of pharmaceutical pollutants is also explored.

2. Properties of NiO Nanoparticles

NiO nanoparticles possess different properties from those of bulk NiO [65–67]. The difference is due to effects such as quantum size and the macroscopic quantum tunnel effect [16,17]. Bulk NiO has a cubic structure with a lattice parameter of 0.4177 nm [68–71]. It is a p-type semiconductor, which is caused by oxygen vacancies, whereby the holes are localized [72,73]. The material has a band-gap value ranging between 3.6 eV and 4.0 eV derived from the 2p to Ni 3D transitions [74–76]. It can be used for a wide range

of applications, such as gas sensors, smart windows, and Li-ion batteries [26,77–80]. In general, the physical and chemical properties of NiO NPs depend on the morphology and particle size [21,77–79]. Bulky NiO has a higher melting point compared to that of nanoparticles [17,18]. For these types of materials, in their usage as photocatalysts, it is important to focus on the hole transport, as it assists in the reduction of unwanted recombination of charge carriers [18]. Also, factors such as oxygen vacancies thus play a pivotal role in terms of the interaction between the nickel (Ni^{2+}) cation and oxygen (O^{-}) anion, which results in structural defects caused by an oxygen-deficient setting [80,81] Below is a structure of NiO (Figure 3) and Table 2, which show its properties.

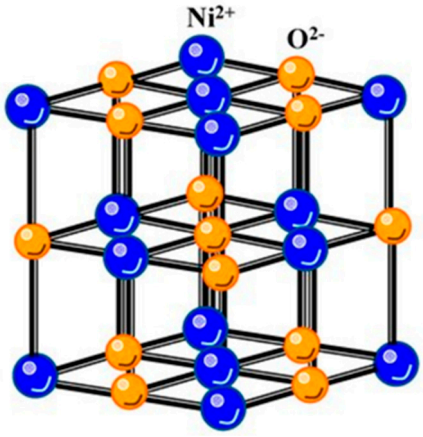

Figure 3. Schematic showing the crystal structure of NiO [81].

Table 2. Properties of NiO [82].

Property	Value
Appearance	Green crystalline solid
Molecular Mass	76.69 g/mol
Density (N) (cm^3)	6.67 g/cm^3
Lattice Parameter (a)	0.4186 nm
Stable Phase at 300 K	3.1–4.3 eV
Conductivity	1.5×10^{-3}
Melting Point	1995 °C
Refractive Index	2.18
Bandgap Energy (Eg)	3.6–4.0 eV
Solubility in water μ (cm^2 Ṇ.s)	0.1–1
a	4.75 Å
b	11.77 Å
c	8.44 Å
B	96°36′

3. Synthesis of NiO Nanoparticles

Several methods have been used for the synthesis of nanoparticles (Figure 4) [82]. The top–down approach involves the breaking down of large materials to form the required nanometric-sized particles. It is conducted through processes like laser ablation, lithography, and mechanical/ball milling [83,84]. In chemical etching, spray chemicals are used in a high-pressure and high-temperature environment to etch and, therefore, form a specific material [85]. With laser ablation, this method is mostly used in the chemical

industry for the synthesis of quantum dots, semiconductors, and carbon nanomaterials. In the biomedical field, it functions for the core-shell synthesis of materials, as these need to be used in drug delivery studies [86,87]. A laser beam is used to remove a specific material from a solid surface and for nanoparticle growth and nucleation, and the usage of vaporized species is also followed. For other methods, such as lithography, certain parts of the materials are used to create a specific pattern during synthesis [88]. Though these top–down methods are able to produce the desired material, their major limitations include huge installation, a large amount of start-up capital, and in most cases, not being suitable for mass production [20].

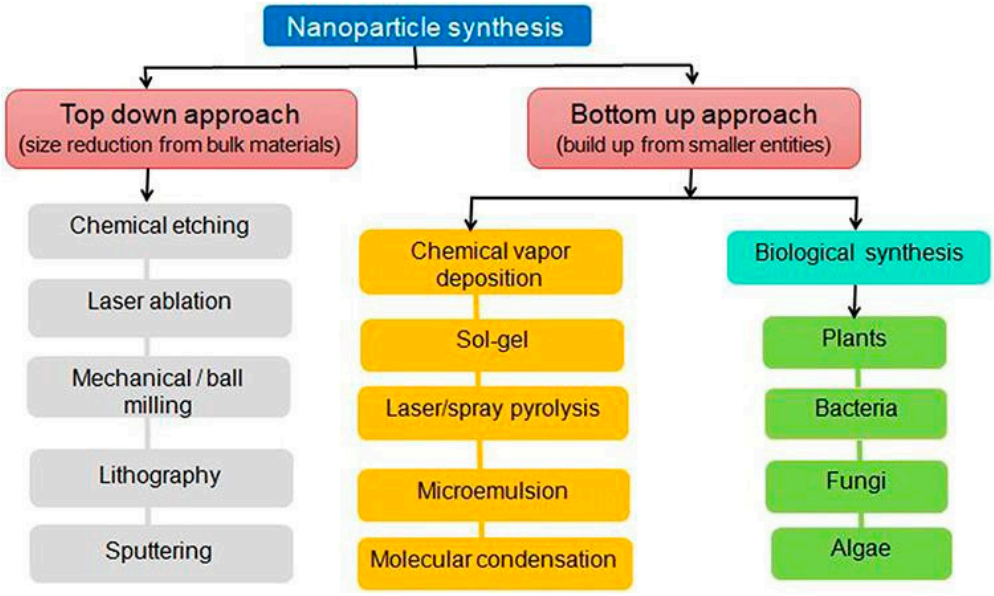

Figure 4. Schematic showing different methods for synthesizing NPs [20].

The bottom–up approach refers to the building up of a material from small particles, such as atoms or molecules. The bottom-up approach is mostly preferred because it is more economical and produces less waste. Some of the well-known bottom-up techniques include sol–gel, molecular synthesis, laser/spray pyrolysis, micro-emulsion and biological synthesis [25].

Different methods have their benefits, as well as limitations and their preferred mechanisms. Many of the above-mentioned methods are restricted for laboratory usage for reasons such high cost, complex mechanisms, and low yield [19].

The sol–gel method includes the usage of chlorides, nitrides, and sulfates to form precursors. These precursors are either dissolved in alcohol or water, and thereafter, a gel is formed from heating and stirring. In that process, the initial small molecules are converted into solid nanoparticle materials. This method can be differentiated into an aqueous sol–gel method and a non-aqueous sol–gel method, but it also involves limitations, such as a large volume shrinkage and cracking during drying [20].

In the co-precipitation method, raw materials are dissolved into the solvent to obtain a homogenous solution, which is then mixed with a base for the precipitate to be formed. Several particles with definitive properties have been formed using co-precipitation. However, limitations have also been noted in the process [89]. These include readjustments of the pH. Continuous washing and drying to achieve maximum purity is a huge disadvantage, as the sample's authenticity might be affected [21]. In another technique, the solvothermal method involves the usage of a solvent under elevated temperature and pressure [22]. The solvent is heated in a closed vessel called an autoclave, where its pressure increases. The

water remains liquid even after it has reached its boiling point. Its major limitation is the need for a long reaction time to complete [22].

The hydrothermal method includes the application of wet-chemical techniques for the crystallization of the material into a nanostructure. It is also conducted in an autoclave with water as a solvent under ambient conditions [90,91]. The difference between solvothermal and hydrothermal is that solvothermal uses organics as a solvent whereas, the hydrothermal method uses water as the solvent [23]. For the hydrothermal method, lengthy response periods spanning several hours can lead to high energy usage [92,93]. Also, the non-uniform temperature results in the formation of materials of varying morphology and sizes [94–97]. In the mentioned methods, the chemical synthesis process has been followed mostly, and because researchers are moving towards environmentally safe materials, more focus has been invested in the green synthesis of photocatalysts [98–101]. Lastly, green synthesis involves the production of nanoparticles using mostly phytochemicals from plant extracts without the usage of toxic solvents or hazardous chemicals [24].

Green Synthesis of NiO and Mechanism of Formation

Green synthesis refers to the environmentally friendly and efficient production of nanoparticles with the aim of decreasing the usage of toxic and hazardous chemicals [24]. This method has received attention due to its economic and safety advantages, as it does not include the usage of harmful chemicals [102,103]. The synthetic process involves the usage of plant extracts, bacteria, algae, and fungi as reducing and capping agents for the formation of metal nanoparticles [27,28].

The usage of plant extracts has been more favored and is shown to be very low in cost, since plants are easily accessible [29]. Plants have shown their ability to detoxify heavy metals that can be used to overcome environmental pollution, such as dye degradation. Plant extracts are not only used as fuels but also as the reducing/capping agents in the synthesis process and are able to reduce metal ions faster than fungi or bacteria. Functional groups such as hydroxyl, thiol, carboxylic acid, amines, and carbonyl groups react with metal ions and are reduced through electrons that flow from the plant extract to the metal in order to activate nucleation. Even though the usage of plants for green synthesis is beneficial, it also possesses limitations such as low yield, agglomeration, reproduction size, unresolved reaction mechanism formation, and shape control during synthesis [30,31].

To understand the mechanism of nanoparticle formation using plant extracts, there are different types of phytochemicals found in plants. These include flavonoids, phenols, saponins, steroids, and alkaloids [32,33]. Secondary metabolites (phytochemicals) of plant and microbial or fungal enzymes are the ones accountable for the reduction of metal ions into metal atoms. In other words, metals in their ionic form can be easily disengaged from their anionic part and be reduced to be stable by using plant extracts. There are several steps that are followed (mechanism) for the formation of nanoparticles using plant extract [33]. Hussein and Mohammed [104], using grapes, showed that the phytochemicals of *Vitis vinifera* were able to reduce Ni^{2+} metal salts into metal NPs. These were conducted by following the stages of activation, development, and termination (Figure 5).

These colleagues noted that, during the activation step, the metal ions are decreased, and the metal atoms are reduced to promote activation. Thereafter, the reduced metal atoms undergo nucleation. In that step, if the reaction rate is faster, the process of nucleation dominates over growth and vice versa. In this nucleation, nickel hydroxide $Ni(OH)_2$ is produced. It can thereafter be easily transformed during synthesis by a thermal decomposition process into NiO. This is accomplished by calcining the reaction to raise its temperature. Consequently, excess moisture or water molecules may be eliminated [33].

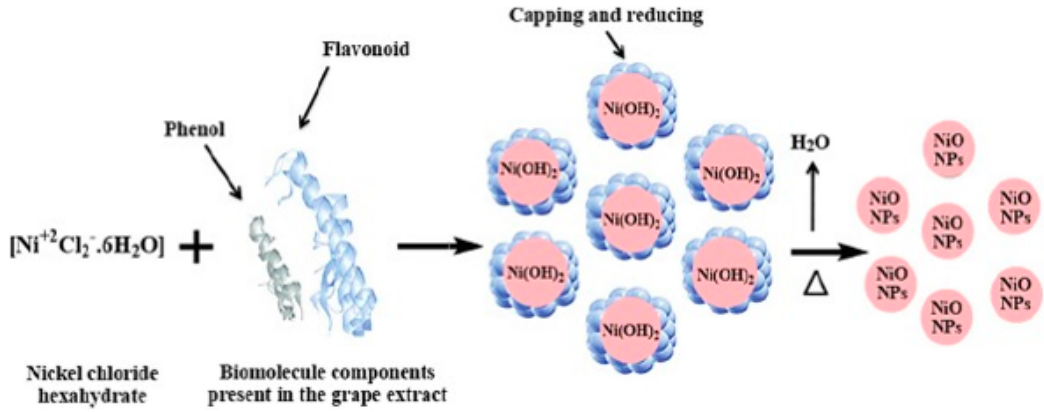

Figure 5. Formation of NiO nanoparticles from grape extract [104] (OA).

In the development step, the ripening of Ostwald occurs, whereby a spontaneous coalescence of small nanoparticles into larger nanoparticles forms. Lastly, during termination, the size and morphology of the nanoparticle are determined. They also noted that, when growth is anisotropic, the size of the NPs increases [77,78,104,105].

Hussain et al. [35] also demonstrated that various metabolites, such as amines and hydroxyls, play a significant role in the bioreduction of Ni^{2+} metal ions to the formation of NiO NPs. Their functional groups', N-H and O-H, role was caused by the strong affinity toward Ni^{2+} metal ions. They postulated that the flavonoids can also change from the enol form to the tautameric keto form upon releasing an active H^+ atom. Moreover, these phytochemicals found in plants can act as surface protectors through electrostatic repulsion [35].

Meena et al. [90], using *Ptelorobium hexapetalum,* which consists of quercetin and caffeic acid, demonstrated that it was possible to convert $Ni(NO_3)_2$ to NiO through complexation. They noted that, in the presence of most plant extracts, the metal ion in the solution tends to precipitate or agglomerate, leading to nanoparticles that are uneven in size and irregularly shaped. In their study using *Pteloribium hexapetalum*, their extracts were able to chelate and stabilize the metal ion by forming coordination complexes (Figure 6). Upon the formation of these complexes, thermal degradation and oxidation occurred during calcination, leading to the formation of well-defined and uniform-sized NiO NPs [90].

Most studies have been shown to use various salts in their synthesis of NiO NPs [90,102]. The effect of salt is known to affect the morphology, crystalline size, and optical properties of the formed NPs. Salts such as chlorides, nitrates, and sulfides have been shown to have a good reduction potential [102,106]. This is caused by the metal centers of the electrons being attached to the electron-donating anions. Thus, the ability to find available electrons from the conjugate salt increases [107–110]. In a study by Louafi et al. [111], the effect of salt concentration using $NiNO_3$ salt was investigated, with an emphasis on nanoparticle sizes. Pure cubic NiO NPs were formed with a particle size ranging from 7–10 nm. From the analysis, as the salt concentration increased, the NP crystallite sizes also increased. The NPs formed using the highest salt concentration of 0.075 M resulted in the highest particle size of 10.7. The increase in the size at higher concentrations may be caused by the high surface energy and tension [112,113].

Ahmad and Kaur [67] synthesized rod-shaped NiO materials using *Coleus scutellariodes* leaf extract and showed the crystalline size to be 23 nm. The maximum UV absorption was found to be 350 nm. The FTIR experiment showed a sharp peak around 464 cm^{-1}, confirming the presence of Ni-O stretching [67]. Feiona et al. [44] synthesized crystalline hexagonal NPs with a minimal size of 21 nm using *Latana camara linn* leaf. From their analysis, UV absorption was noted around 245 nm, and a minimal shift toward a higher wavenum-

ber was seen, which suggested a decrease in the band-gap value [44]. Bekele and Mahammed [40], using a leaf from *Vernonia amygdalia,* formed octahedral-structured material. Uddin et al. [42] synthesized rhombohedral-shaped materials from *Berberis balochistanica* plant extract. Haides et al. [46] using *Zingiber officinale* and *Allium sativum* (roots), showed UV absorption at around 275 nm for ginger and 280 nm for garlic, with bandgaps of 3.1 eV for ginger and 3.0 eV for garlic for the spherical- and agglomerated-shaped NPS. The average crystalline size was found to be 33 nm for ginger and 30 nm for garlic, and the broad peaks on the XRD indicated that there was a presence of phytochemicals of garlic and ginger extracts acting as capping agents [46].

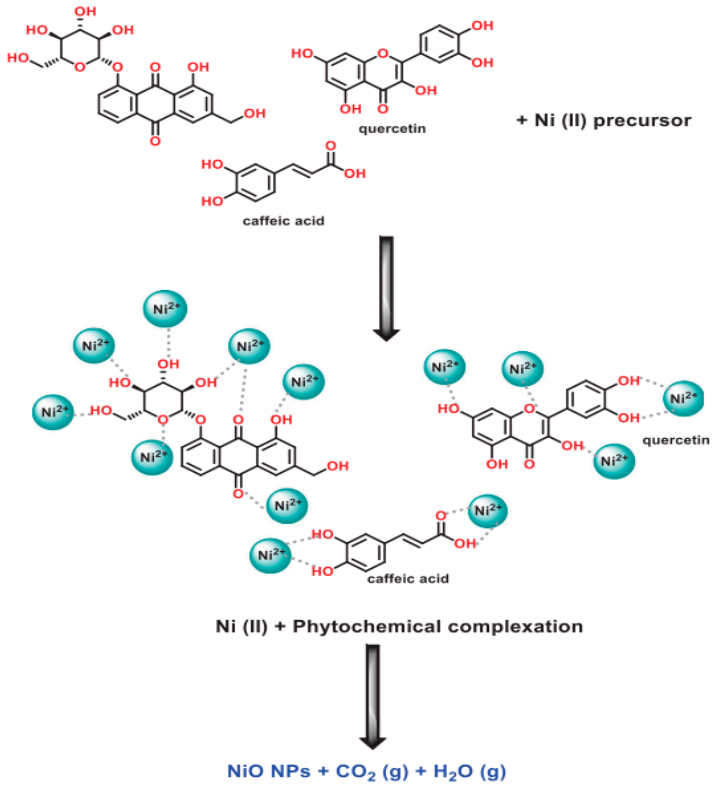

Figure 6. Mechanism of formation for *Ptelorobium hexapetalum* [90].

As noted in the studies above, different compounds are able to synthesize various NiO particles, producing various physical and optical properties. The synthesis of nanoparticles using plant extracts is mostly influenced by the phytochemicals found in the plant and the synthesis conditions. When plant extracts are used, compounds consisting of phenolics (chlorogenic acid) and flavonoids (kaempferol-3 glucoside, quercetin, and aphthadiathrones) are used as reducing agents. For a compound to act as a reducing agent, it requires an enol group, and for a capping agent, a methyl group is needed. If both groups are present, the compound can perform a dual role of reducing and capping. From various studies, it has been noted that phytochemical compounds that have an ortho-substituted hydroxyl can result in small particles with a specifically defined shape. In the study reported by Reddy and Lashmikanth [38] these authors used *Azadirachta indica*, *Morinda citrifolia*, and *Terminalia elliptica* leaf extracts for the synthesis of large grains of nanoparticles with various morphological facets and spherical-shaped materials with a uniform distribution and small particle size, respectively (Figure 7). The *Azadirachta indica*-mediated NiO NPs formed facets with large-grain clusters, and this morphology differed compared to the other formed materials. This could be due to the compounds of limbin and limonoids found in this compound, which were absent in *Morinda citrifolia* and *Terminalia elliptica* plant extracts. For the *Morinda citrifolia*- and *Terminalia elliptica*-mediated NiO NPs, uniform

smaller particle sizes and spherically shaped NPs were formed for both materials. In these compounds, common phytochemicals were identified, including short-fatty acids, lignans, carotenoids, flavonoids found in *Morinda citrifolia*, and the general compounds (lignans, tripenes, tannins, polyphenols, and flavonoids) identified in *Terminalia elliptica* [35]. These common compounds with their reaction conditions could have influenced the formation of spherical materials as compared to the facets. Also, the formation of spherical materials is highly reported in Table 3, as most compounds contain the reported phytochemicals from their compounds.

Khan et al. [47], using *Abutilon indicum* leaf extract, produced agglomerated NPs with an absorption of 330 nm. These materials were noted to be redshifted compared to the previously reported studies of green NiO. This redshift may have been caused by the transfer of non-bonding electrons assisted by the phytochemicals. Noukelang et al. [50] also formed agglomerated quasi-spherically shaped NPs from *Rosemarinus officinalls*. The materials had a particle size range of 12–16 nm and a bandgap of 3.39 eV. Moreover, from FTIR, a strong band at around 569 cm^{-1}, indicating the presence of NiO metal oxide, was noted [50]. Ramesh et al. [56] synthesized porous-shaped NiO NPs using *Plectranthus amboinicus*. A material with a UV absorption of 320 nm and a bandgap of 3.6 eV was formed. The FTIR showed vibrations of C-N and −OH stretching, which corresponds to the presence of the Ni-O [56].

A flower-shaped NiO NP using *Capparis decidua* leaf extract with a crystalline size of 16.75 nm was produced. The maximum UV absorption for the NiO nanoparticles was found to be 410 nm. Also, the presence of proteins deduced from the plant was recorded through the FTIR peaks, which showed the presence of the -COOH group and N-H stretching in the amino acids [58]. Baytar et al. [64] used a watermelon seed to form triangular NiO NPs with a crystallite size of 7 to 20 nm. The absorption was found to range between 199 nm and 298 nm with a bandgap of 3.62 eV [64].

Bhoye et al. found *Gymnema sylvestre* leaf extract-synthesized oval and pseudo-spherical NiO NPs with a crystalline size of 25 nm [68]. The FTIR vibration showed the −OH group and C=O and C=C groups, which confirmed the presence of phenolics, flavones, tannins, and aliphatic acids, which were responsible for reducing the metal precursor. A maximum UV band was observed at 289 nm with a 4.29 eV bandgap [68].

Meena et al. [90] using *ptelorobium hexapetalum*, formed homogeneous clusters of mostly spherical (Figure 8c,e) NiO NPs, and this formation was confirmed using EDS (Figure 8d) and SAED (Figure 8f). They also used Raman spectroscopy to confirm the presence of Ni^{++} in the phonon and magnon regions and the defect content of the materials. Through TGA (Figure 8b), they were able to understand how thermally stable the formed materials were, as they noted decomposition related to the conversion of the $Ni(OH)_2$ to NiO, which occurred between 294 °C and 350 °C during the calcination step. Lastly, from a BET analysis (Figure 8a), a mesoporous structure with a surface area of 89 m^2g^{-1} was noted. This is of significance, as these materials are highly porous. And the added active sites can assist in the degradation efficiency of this green-synthesized material.

From Table 3, it can be noted that different parts of the plants (leaves, fruits, roots) were used for the synthesis of various NiO NPs. Most of these, possess the spherical morphology though other morphologies were also noted such as cubic, flower-shaped, rods, octahedral, sheets, triangular, and oval. Varying sizes, mostly in the range of 8–60 nm were also reported indicating the materials to be of nanometer range. The optical characteristics mostly reported a bandgap around 2.9–3.2 eV and around 300 nm wavenumber. The excitations around 300 nm for green NiO are mainly caused by charge transfer in the NiO lattice as there is a transition from the O^{2-} to Ni^{2+} ions. Although reports from studies such as Meena et al. [90] showed that controlled morphology could be formed. It was noted that

more needs to be done to study these green inorganic materials, as factors such as the effect of pH, plant concentration, calcination temperature and use of various phytochemicals could play a role in the formation of distinct and uniform nanoparticles.

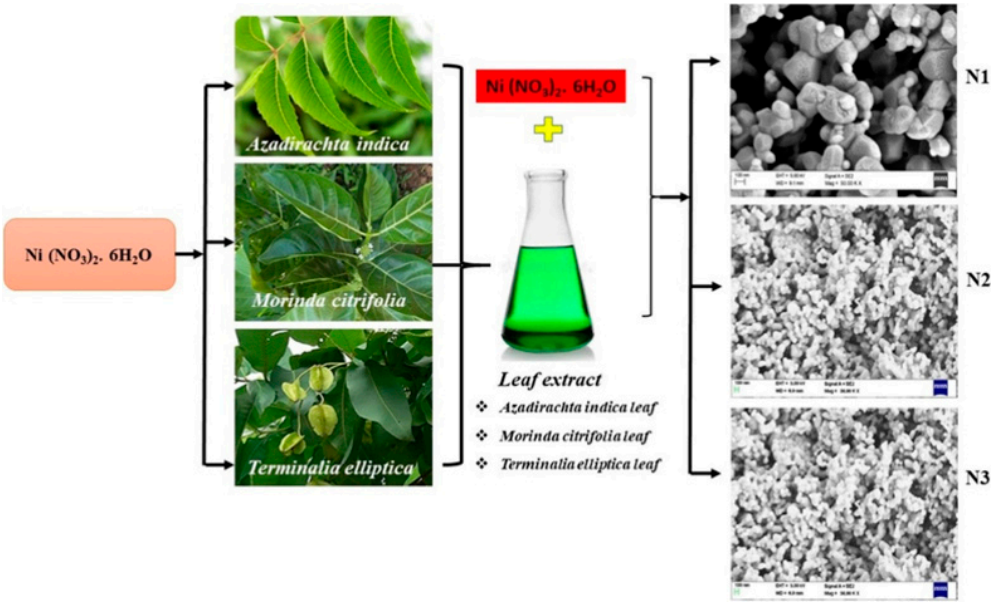

Figure 7. Process of green synthesis NiO nanoparticles using plant extracts [38] OA.

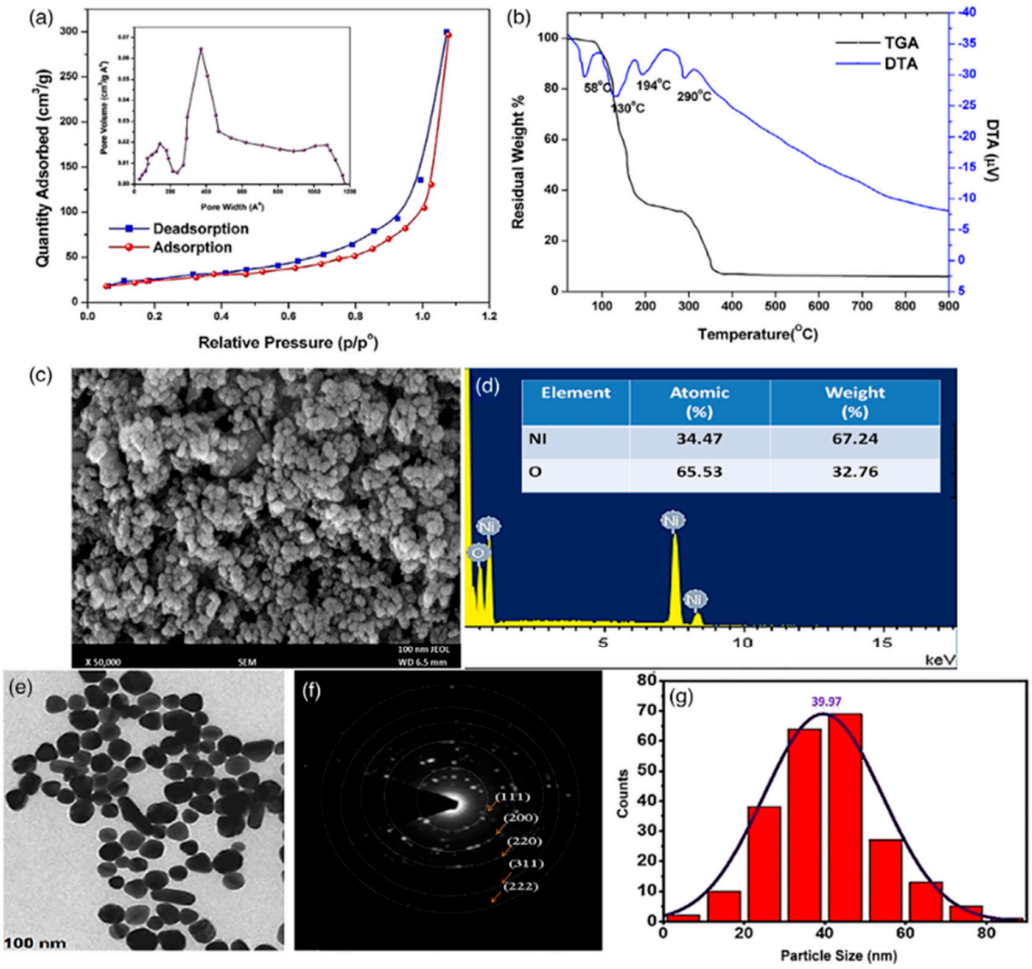

Figure 8. (**a**) Surface area, (**b**) thermal stability, and (**c**–**g**) morphological studies of *Pterolobium hexapetalum* flower extract mediated NiO NPs [90].

Table 3. Morphological and optical properties of plant-derived NiO.

Plant (Family)	Size (nm)	Shape	Optical Properties	Refs
Sutherlendia frutescene	18.4	Flowerlike	302 nm, 3.5 eV	[21]
Aegle marmelos	8–10	Spherical	355 nm and 3.5 eV	[33]
Moringa oleifera	20–50	Spherical oval	305 nm	[34]
Acacia nilotica	16	Spherical	-	[35]
Hydrangea paniculata	33	Spherical, Oval, and Rod shaped	-	[36]
Buxus wallichiana	24.2	Spherical	1.99 eV	[37]
Azadirachta indica	96.95	Spherical	879 eV (XPS)	[38]
Eucalyptus globulus	19	Agglomerated	406 nm	[39]
Vernonia amygdalina (leaf)	17.86	Octahedral	-	[40]
Arabic gum (gum)	43	Spherical and agglomerated	280 nm and 3.3 eV	[41]
Berberis balochistani (steam)	31.44	Rhombohedral agglomerated	305 nm	[42]
Opuntia ficus indica (leaf)	16.01	Spherical	-	[43]
Latana Camara linn (leaf)	21	Hexagonal	245 nm	[44]
Rhamnus triquetra (leaf)	25	Spherical	333 nm	[45]
Zingiber officinale and *Allium sativum* (roots)	Ginger—32.9 Garlic—29.92	Spherical	350 nm, 3.1 eV for ginger, and 3.0 for garlic	[46]
Abutilon indicum (leaf)	-	Cubic and agglomerated	330 nm	[47]
Areca catechu (leaf)	5.63	Hexagonal and Rhombohedral	380 nm	[48]
Eichhornia crassipes (leaf)	33 nm (XRD) 60 nm SEM	Spherical	357 nm	[49]
Rosemarinus officinalis (leaf)	15.5	Quasi-spherical shaped	365 nm and 3.39 eV	[50]
Raphanus sativus (root)	22.37	-	346 nm and 2.8 eV	[51]
Calendula officinalis (leaf)	16.9–43.9	Spherical	325 nm (PL)	[52]
Leucas aspera (leaf)	40.438	Spherical	-	[53]
Limonia acidissima (fruit)	21	Spherical	3.8 eV	[54]
Stevia (leaf)	13.7	Spherical	2.7 eV	[55]
Plectranthus Amboinicus (leaf)	41.8	Agglomerated porous shape	320 nm and 3.6 eV	[56]
Nigella sativa (seed)	20	Spherical and agglomerated	317 nm	[57]
Capparis decidua (leaf)	16.75	Flower shaped	410 nm	[58]
Allium jesdianum (leaf)	20.80	Spherical	390 nm	[59]
Punica granatum (peel)	26.1	Porous honeycomb structure	348 nm and 3.63 eV and 2.54 eV	[60]
Clitoria ternatea flower	9.6	Hexagonal	283 nm and 2.24 eV	[61]
Cleome simplicifolia	7	Spherical	2.75 nm and 4.38 eV	[62]
Rosemary plant shoots	19	Quasi-spherical	-	[63]
Watermelon seed	33	Triangular shaped	199–298 nm and 3.62 eV	[64]
Commelina Benghlensis	30.58	Spherical	309 nm and 3.8 eV	[65]
Allium stativum	22.12	Petal flower-shaped and spherical	2.9 eV	[66]
Coleus scutellarioides	23	Rod	350 nm	[67]
Gymnema sylvestre	25	Oval and pseudo-spherical	288.9 nm and 4.29 eV	[68]
Psidium guajava	23	Agglomerated	2.58 eV	[69]
Calotropis gigantea	60	-	415 nm and 3.6 eV	[70]
Aloe vera	15.4	-	3.28 eV	[71]
Ptelobium hexapetalum		Spherical clusters	373 nm	[90]

4. Plant-Derived NiO as a Photocatalyst

One of the most preferred treatment methods is the photocatalysis method as it can degrade pollutants without producing harmful by-products. Unlike other treatment methods, photocatalysis uses clean energy sources such as sunlight or low energy-consumption lamps. The photocatalytic process uses oxidizing species such as hydroxyl radicals to degrade organic dyes [75,114].

The green synthesis of nickel oxide (NiO) nanoparticles has gained popularity in their effectiveness in the degradation of various organic dyes. These green-synthesized NiO nanoparticles exhibit exceptional catalytic capabilities in degrading harmful organic dyes such as methyl orange (MO) [87], Congo red (CR) [83,85,88], crystal violet (CV) [115], methylene blue (MB) [82,84,89], acid orange 7 (AO7) [86] and fast green (FG) [90]. These NiO nanoparticles have shown high efficiency between ~73–100% in dye degradation.

Shubha et al. [5] used sheep dung-mediated NiO in the presence of UV and Visible light for the degradation of MB and MG dye pollutants. After 100 min, a 99% and 98% degradation efficiency was recorded using UV light, at optimum conditions of 15 mg, 4 ppm, and pH 7. The materials could be reused up to 3 times with an efficiency above 88%. Motene et al. [21] also with flowerlike NiO NPs, with a bandgap of 3.5 eV, managed to degrade 89% and 98% of MB and MG respectively. The materials could be reused up to three times with high efficiency [21]. Prabhu et al. [61] with hexagonally shaped NiO materials, were able to degrade 89% and 76% of FG and RB respectively (Figure 9a–d) using solar sunlight [61]. The low bandgap of 2.2 eV and minimal particle sizes of 13 nm may have contributed to the increased degradation rate. A pseudo-first-order degradation (R^2—0.89 and 0.93) with specific reaction rates (0.032 and 0.022) was also recorded which obeyed the Langmuir Hisselwood model.

Sabouri et al. [76], using *Salvia macrosiphon* Bioss plant-mediated NiO, tested their materials against MB for degradation in the presence of UV light, where the effect of pH (4, 7, and 9) was investigated. The highest degradation was recorded at pH 9, with an 89% efficiency, and the lowest was recorded at pH 4, with 39%. The authors noted that highly reactive OH radicals played a major role. The photocatalytic mechanism showed that the existing electrons in the valence band were excited by the conduction band of oxide, along with the formulation of holes in the valence band to form an electron–hole pair. The obtained hydroxyls were used for the dye degradation. Some of the hydroxyls were formed through the disintegration of water. It is known that, upon degradation, different dyes produce different products. For example, some of the byproducts such as the aromatic amine and phenolics are produced from the degradation of synthetic dyes and antharoquinones, respectively. Also, depending on the structure of the dye, carboxylic acids might also be present. However, when completed, degradation has taken place, and CO_2, H_2O, and a few organic ions should form. It is not always the case, and hence, authors have moved towards the use of HPLCMs for the identity of the compounds present after degradation.

Subashini et al. [116], using green NiO from *Sterculia foetida* leaf, were also investigated. Under UV irradiation, the degradation of MB was observed at 15 min intervals for an hour. Thereafter, a high photocatalytic activity of MB (98%) was noted. Roopan et al. using the Box–Benken statistically designed cuboidal NiO NPs with a particle size of 28 nm, were able to degrade 95% of CR dye in the presence of sunlight in 40 min [83]. Khan et al. [88] using *Tribulus terrestris*, managed to synthesize spherically shaped NiO materials with no aggregates and small sizes. From their analysis, they were able to degrade 100% of Congo Red dye (CR) in less than 30 min [88]. Also, Sundaresan et al., using *Evolvulus*-mediated NiO, managed to degrade more than 85% of the RhB dye in less than an hour [99].

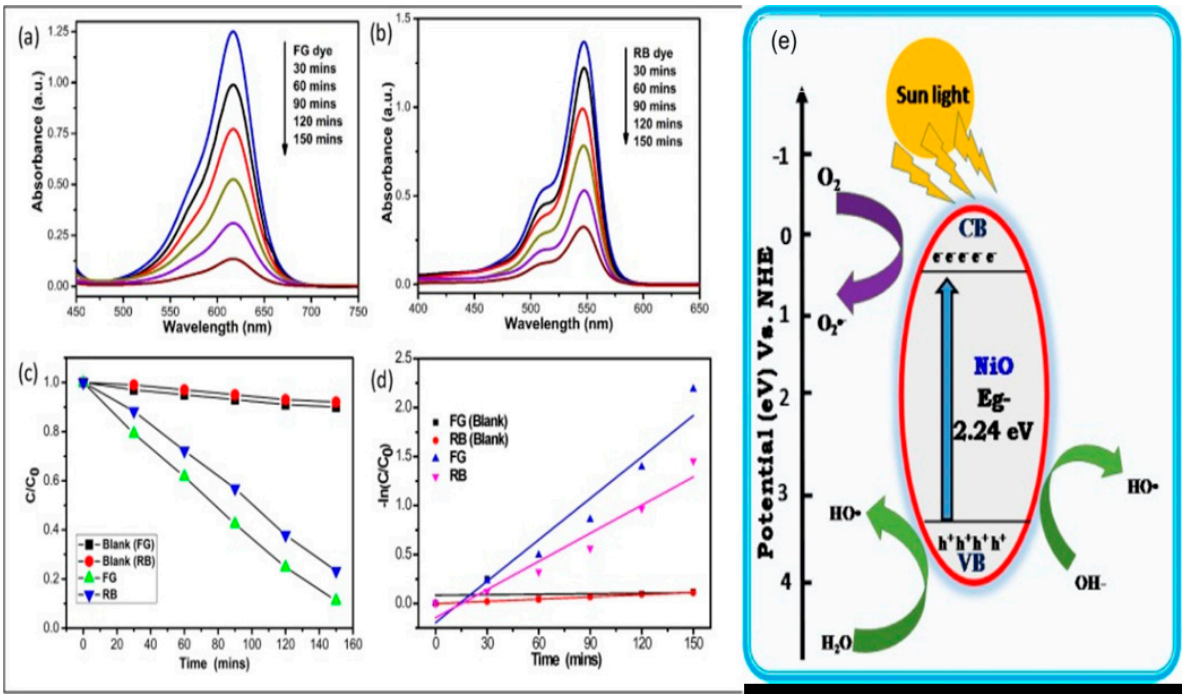

Figure 9. (**a**,**b**) UV plots showing FG and RB degradation, (**c**,**d**) kinetics studies of FG and RB, and (**e**) mechanism of degradation [61].

Therefore, green synthesis methods for nickel oxide (NiO) nanoparticles are highly effective at degrading various harmful organic dyes, achieving high degradation efficiencies owing to their superior photosensitivity, great durability, and exceptional optical properties [83,99,116].

The application of NiO nanoparticles, including in composite forms, has shown significant promise in enhancing photocatalytic performance for environmental remediation.

From Table 4, different pollutants were used with different photocatalysts, resulting in differences in degradation efficiency percentages. Several studies were able to achieve a degradation of 90% and above in a time frame of 30 min or less. These studies used mostly UV light and a catalyst dosage of 10 mg and higher. Variables such as pH, pollutant concentration, and pollutant type did not have a significant effect on the trend observed. Also, another factor that could play a role in terms of how degradation takes place is the material size. The effect of material size plays a major role in how a photocatalyst degrades. Small-particle-sized materials generally have a large surface area, and that assists in the dispersion of the particles and how the rate of the reactions is affected. Khatun showed that a big particle size resulted in a low surface area, which later reduced the density of the active site on the catalyst surface. From Table 4, studies that recorded a high reaction rate in terms of degradation efficiency (90% and above) and minimal reaction time (less than 1 h) showed there was no direct correlation in terms of particle size and efficiency. As noted in studies by Mandal et al., which had materials in particle size ranges between 13 and 40 nm recorded the highest efficient degradation rate of 96% in 0.01 h [60]. Their high degradation rate could have been due to the low bandgap (2.72 eV) they recorded, which meant that the amount of energy required to excite the electrons was less and the rate of recombination was less. Byat et al., also with a particle size of 33 nm, had a degradation of 98% at 0.2 h [64]. Barzyin et al. [87] and Khan et al. [88], with materials of particle sizes of 25 nm and 60–90 nm, also had high degradation efficiencies (above 90%) in short periods of time against various pollutants, such as MO and CR dye. From these studies, it is clear there is no singular factor that can influence how degradation can occur. Hence, in most

studies, researchers gravitated towards studying the effect of variable factors (time, pH, concentration, dosage, and pollutant type) to obtain the preferred optimum conditions for that particular material. Also, the bandgap, particle size, plant concentration, and morphology play a role.

Table 4. Green NiO against different organic pollutants.

Reductant	Organic Pollutant	Degradation Conditions (pH, Dosage, Conc, and Light Source)	Efficiency (%)	Radiation Time (h)	Refs
Sheep dung	MB	pH 7, 15 mg, 4 ppm	99	1.67	[5]
Sutherlendia Frutescence	MG & MB	pH 7, 20 mg, 20 ppm, 150 W UV light	89, 92		[21]
Arabic gum	MB	pH 9, 10 mg/L, 100 mL, UV light	82	4.5	[41]
Lantana camara	MB	0.01 g, 0.2 L, UV light	85	2	[44]
Punica Granatum	MO	50 mg, 25 mL, 0.25 mg	96	0.01	[60]
Clitoria Ternatia	FG	25 mg, 25 mL, 20 ppm, Sunlight	89	2.5	[61]
Watermelon	MB	50 ppm, 10 mg, UV light	98	0.21	[64]
Commelina benghalensis	MG	pH 3, 30 mg and 5 ppm, UV light	95	2	[65]
Salvia macrosiphon Bioss	MB	pH 9, 3 ppm, UV light (11 W)	89	5	[76]
Citrus Fruit Juice	EB	50 mg, 100 mL, sunlight	91	2.5	[117]
Sterculia foetida	MB	1 mmol, 100 mL, 15 mg, UV light	98	1	[116]
Senna auriculata	MB	pH 8.5, 0.2 g/L, 10 mL, Vis Light	97	1.5	[82]
Calotropic gigantea L.	CR	0.1 g, 100 mL, 10 mg/L, Sunlight	95	0.58	[83]
Hordeum vulgare	MB	pH 12, 20 ppm, 0.1 g	>95	1	[84]
Annona muricata L.	CV	50 mg, 50 mL, 20 mg/L, Sunlight	99	1.75	[115]
Allium cepa	CR	pH 6, 0.003 g/L, 5 mg	90	1.5	[85]
Bierberstenia multifida	AO7	pH 7, 1 g, 1 g	90	2.7	[86]
Punica granatum L.	MO	0.1 g, 50 mL, 10 mg/L	>90	0.62	[87]
Tribulus terrestris	CR	10 mg, 50 mL, UV light	100	0.5	[88]
Azadirachta indica	MB	pH 11, 60 mg, 10 mg/L	73	0.5	[89]
Ptelorobium hexapetalum	MB	10 mg/L	89	2.5	[90]
Pisonia alba	MB	pH 6, 0.1 g/L, 1×10^{-5} M	77.7	1	[91]
Tragacanth	MO	74 mg, 100 mL, pH 9, UV light	82	3.5	[92]
Hilliardiella hirsuta	MB	1 mg, 50 mL, 5 mg/L, pH 10	97	2	[93]
Portulaca oleracea	MB	10 mL, 2.5×10^{-5} M, UV light	65.5	1.67	[94]
Clerodendrum phlomidis	MB	20 mg, 20 mL, 2.0×10^{-5}, UV light	92	1	[95]
Tectona grandis	XO	10 mg/L, 5 mg/L, UV light	98	1.67	[96]
Cydonia oblonga	RhB	3.7 mg, pH 9, 50 mL, UV light	79	1.5	[97]
Phyllathus niruri L.	MB	20 mg, 5 ppm	100	3 h	[98]
Evolvullus alsinoides	RhB	20 mg, 20 mL, UV light	85	0.67	[99]
Piper betle	RR141	50 mg/L, 15 mg, Vis light	99	1.67	[100]
Justicia adhatoda	MB	100 mL, 20 mg/L, UV light	94	1	[101]

MB—Methylene Blue; CR—Congo Red; Methyl Orange (MO); FG—Fast Green; RB—Rose Bengal; RhB—Rhodamine Blue; RR141—Reactive Red 141; AO7—Acid Orange 7; EB—Evans Blue Dye.

As noted in Table 4 and Figure 10, there are a lot of dyes that are emerging due to the different applications they are used in, and this has prompted researchers to work towards a better understanding of these pollutants. As shown previously, for example, if the dye concentration is too concentrated, the surface of the NiO can become saturated. Also with pH, it is directly related to the surface charge of the NPs, which can influence the adsorption ability of the material. Thus, when the NiO material interacts with the dye, factors such as radical regeneration, charge transfer, degradation, and adsorption are taken into consideration. During the process, the dye will be absorbed on the surface of the NiO. Thereafter, it will interact with the formed radicals during photocatalysis, resulting in the degradation of the particles, and these efficiencies are mostly influenced by the surface area, pH, and electron attraction.

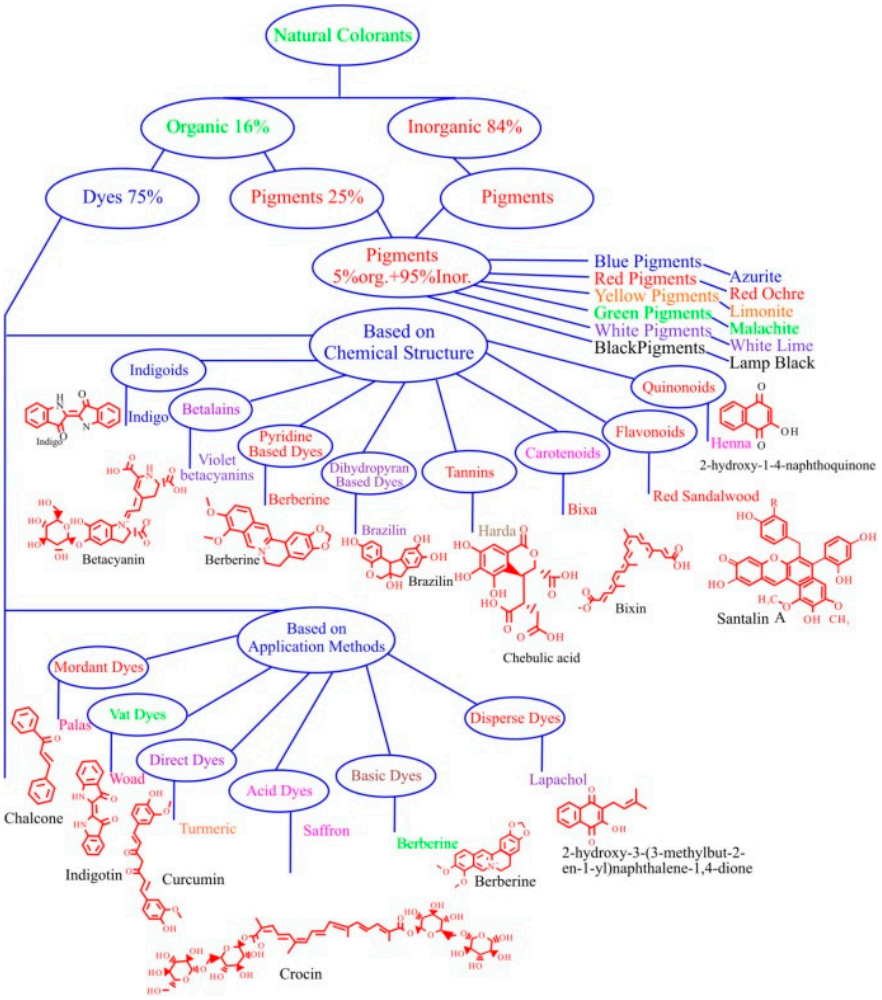

Figure 10. Classification of dyes and pigments [118].

5. Limitations of NiO as Photocatalysts and Modification

Researchers have found the use of monometallic nanoparticles, such as NiO, to have limitations, which include them being less specific and becoming rapidly deactivated [119]. To avoid the mentioned limitations, several modifications have been conducted, and these include modifying ligands with functional groups, constructing heterogeneous junction composites, doping metal nodes, and adding co-catalysts [120]. Heterojunction formation helps in increasing electro-conductivity and decreasing the bandgap. When two bands of different semiconductors are brought into close contact, an electric field is produced, and the difference in their band potentials creates charge separation, which causes an e^- transfer between them [121]. However, heterojunction formation can also have its limitations in photocatalytic reactions. It has been noted that there tends to be a slow transfer rate of gaseous reactants, which allows the generation rate of reactive oxidation species [122,123]. Thus, several authors are also interested in the direct bimetallic formation of composites. Researchers have opted for bimetallics because they improve the physical, electrical, magnetic, and catalytic properties of monometallic nanoparticles. Bimetallics include a combination of two different metals with enhanced reaction properties and characteristics [72,73]. Bimetallization causes a decrease in the particle size. The decrease in particle size increases the surface-to-volume ratio, which increases the number of active sites, making the energy barrier low, thus causing an increase in catalytic activity [74]. Several studies have been conducted in an effort to improve the activities of green-synthesized NiO materials. The

activity of these bimetallics has been influenced by several factors, including the reductant used, radiation time, degradation conditions, pollutant of interest, and its concentration.

Legmairi et al. used *Portulaca oleracea* to form NiO-decorated Fe nanocomposite for the degradation of MB using sunlight [94]. An improved degradation efficiency was noted after loading the Fe^{3+} cations, as the bandgap and recombination rate were reduced. This may have been prompted by the introduction of traps for holes and electrons. Puttaraju et al. studied the mixed metal oxide-based nanocomposites (ZnO/NiO NCs) for the degradation of MB dye [98]. The study concluded that ZnO/NiO NCs synthesized using *Phyllanthus Niruri* (L) with a bandgap of 3.11 eV showed promise for diverse applications, as it degraded 100% of the MB in 180 min [98]. Also, electrons were found to be the species responsible for the MB degradation. Singh et al. [101], utilizing *Justicia adhatoda* leaf extract as a reducing and capping agent in a green synthesis of NiO/ZnO nanocomposites (NCs), managed to degrade ~94% of MB under UV light.

Several studies also showed the usage of Cu as a dopant or for the formation of heterostructures. The Cu material for photocatalytic reactions is known to increase the active site count. Bavaji et al. in their studies stated that Cu ions reduce the recombination of the electron–hole due to the large energy band [124]. They stated that this leads to a large number of free electrons and holes assisting in the formation of free radical ions. Kalita et al. formed various bimetallic CuNi ratio (1:1, 3:1, and 1:3) materials using peppermint leaf extract (Figure 11a–i) [119]. They studied the effect of these bimetallics over an azo dye (CR), a cationic dye (MG), and a heterocyclic dye (MB). Upon testing the degradation, it was noticed that CN11 produced the highest efficiency, with a 100% degradation after 25 min (Figure 9a,d). The other two materials, CN 31 and CN13, only managed efficiencies of >80% after 40 min and 75 min, respectively [119]. Bavaji et al. used phytolacca dodecandra-loaded ratios of 1%, 3%, and 5% of Cu on NiO for improved degradation [124]. In the presence of UV light, after 1 h, the 5% CuNiO recorded the highest degradation, of 99%, towards MB, with a rate constant of 0.9871 min^{-1}. Moreover, the materials could be reused several times while maintaining a high degradation efficiency [124].

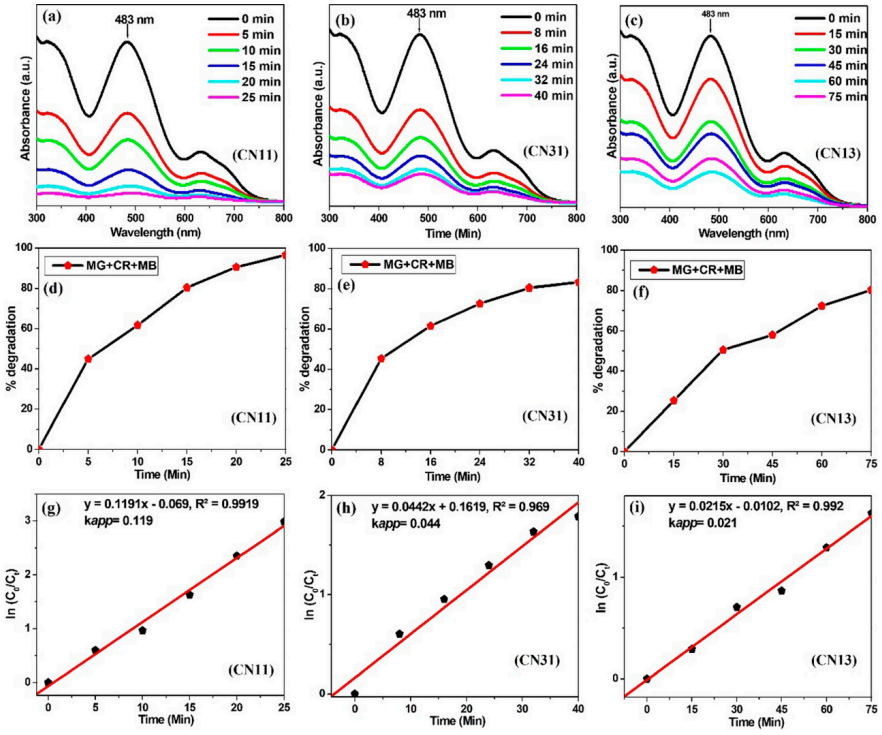

Figure 11. (**a**–**c**) UV plots, (**d**–**f**) percentage degradation, and (**g**–**i**) kinetic plots of various CuNI bimetallic against various dyes.

From these studies (Table 5), it could be noted that high degradation rates (>80%) were observed in almost all of the studies, with mainly shorter times compared to the bare NiO. A mixture of UV, visible, and sunlight was used. The effect of the variables also played a role in the efficiency. Lastly, the effect of doping or the formation of heterostructures played a major role, as the rate of recombination was slowed down. Also, the reduced bandgap in most of the composites proved that less energy was required to produce radicals, which could be used for the degradation of these dyes in water.

Table 5. Photocatalytic activity of green-synthesized nickel-based bimetallic.

Modification	Reductant	Organic Pollutant	Degradation Conditions	Efficiency (%)	Radiation Time (h)	Refs
Fe/NiO	*Portulaca oleracea*	MB	2.5×10^{-5} M MB, sunlight	66	2	[94]
ZnO/NiO	*Phyllanthus niruri*	MB		100	3	[98]
NiO/ZnO	*Justicia adhatoda*	MB	UV light,	94	1	[101]
CuO/NiO	*Mangifera indica* L.	Glyphosate	6 mg, 25 mL, pH = 7, UV-light	71.23	5	[122]
Cu-Ni	*Mentha piperita*	MG, CR, MB	30 mg/L, 20 ppm, Sunlight	99.5	0.4	[119]
Cu-NiO	*Lycopodium Linn*	MB	50 mL, 0.03 g, pH = 9, sunlight	99	1	[124]
Cu-NiO	*Phytolacca dodecandra*	MB	100 mL, 20 mg, sunlight	97.98	2.7	[125]
Cu-Ni	*Dypsis lutescens*	RhB	25 mL, 20 mg, tungsten lamp	91	1.7	[126]
Cu-Ni/GP	*Ginger Rhizome*	RhB	0.5 mL, 3 mL, 10 mg	97	0.1	[127]
ZnO-NiO	*Clitoria ternatea*	CV	25 mL, 24 mg, sunlight	84.4	2.5	[128]
Fe-Ni	Eucalyptus	MO	1000 mL, 10 mg/L, 0.5 g/L	99.6	3	[129]
Ag-Ni	*Zingiber officinale*	Safranin O	40 mL, 8 mg, UV radiation	~100	0.5	[130]
Fe-Ni	*Carica papaya*	O G	1000 mg/L, 1 g/L	97–99	1	[131]
CuNi	*Saccharum officinarum*	MB	5 mg, 20 mL, UV radiation	98	3	[132]
Ag/Pd/Ni	*Cassia auriculata*	Safranin O	50 mL, 0.010 g, UV (mercury lamp) radiation	98	0.4	[133]
CuO/NiO	*Carissa edulis*	CR	50 mL, 30 mg, visible light (Xenon lamp)	82	1.5	[134]
Ag@Ni	*W. coagulans*	MO	50 mL, pH = 8, 5 mg/L, sunlight	82	1.3	[135]
Ag-Ni-Mn-Zn	Watermelon seeds	MR	5 mL, 1 mg, UV light	97	1	[136]
NiO/ZnO	*Justicia adhatoda*	MB	100 mL, 0.8 mg/mL, UV light (Hg vapor lamp)	97	1.5	[137]
Pt-Ru-Ni	Wood chips	MB	10 mg, 1 mg, visible light	97	5	[138]
Cu-NiO	*Commelina benghalensis*	MG	100 mL, 25 mg, UV light	97.69	0.75	[139]
Cu-Ni	*Terminalia chebula*	CR	50 mL, 5 mg, 50 ppm	99.6	0.25	[140]
Fe-Ni	*Pithecellobium dulce*	GW MR	0.5 mg, 10 mg, pH = 7	70	2	[141]

MG—Malachite Green; CR—Congo Red; MB—Methylene Blue; MO—Methyl Orange; S O—Safarin O; OG—Orange G; GWMR—Golden Yellow MR.

6. Degradation of Pharmaceuticals Using Green NiO and Its Composites

The degradation of pharmaceuticals in the environment is a critical issue due to their persistence and potential toxicity [110]. Traditional wastewater treatment processes often fail to fully remove these contaminants, leading to their accumulation in water bodies and the soil. Advanced oxidation processes (AOPs), including photocatalysis, are emerging

as effective methods for degrading pharmaceuticals. Emerging in the last decade have been pharmaceuticals such as Ciproflaxin (CIP), Sulfisoxazole (SSX), and Sulfamethoxazole (SMX), as well as their usage in varying medical applications, in particular as antidepressants and for the treatment of infections. Green NiO and NiO heterostructures have also been tested for their efficiency against these pollutants in waters, and in Table 6 are some of the studies that have been conducted.

Table 6. Photocatalytic activity of green-synthesized photocatalysts against pharmaceutical pollutants.

Photocatalyst	Reductant	Organic Pollutant	Degradation Conditions	Efficiency %	Reaction Time (h)	Refs
NiO	*Araucaria columnaris*	Carbamazepine	Sunlight irradiation, 5 mg/L, pH = 4	99	2.25	[142]
NiO	*Araucaria columnaris*	Naproxen	Sunlight irradiation, 5 mg/L, pH = 4	98	2.25	[142]
NiO	*Aegle marmelos*	4-chlorophenol	UV light (mercury lamp), 100 mL, pH = 8	87	3.5	[6]
NiO	*Calotropis gigantea latex*	4-nitrophenol	Sunlight, 50 mL, 50 mg	94	0.83	[107]
NiO/rGO	*Pometia pinnata*	Tetracycline	UV-Visible (100 W Xenon lamp), 0.2 g, 250 mL	99	0.5	[106]
rGO-NiO/CdO	*Alternanthera sessilis*	Phenol	UV (100 W incandescent bulb), 100 mg/L, 6 mg/L	89.6	1.5	[108]
CuO-NiO-HNT	*Carissa edulis*	Tetracycline	Visible light (300 W Xenon lamp), 20 ppm, 30 mg	84	1.5	[109]
$Zn_{0.5}NiO_{0.5}FeCrO_4$	*Tragacanth gum gel*	4-nitrophenol	Visible light (Fluorescent lamp), 50 mL, 10 mg/L	80	2.5	[143]
$Zn_{0.5}NiO_{0.5}FeCrO_4$	*Tragacanth gum gel*	Aniline	Visible light (Fluorescent lamp), 50 mL, 10 mg/L	95	3	[143]
NiO doped CuO	*Allium staivum*	Ciprofloxacin	UV irradiation, 10 mg, 250 mL	68	2.91	[107]
Chit-Cell@Ni/NiO	Barley and shrimp	Ciprofloxacin	Sunlight, 50 mL, 10 mg/L, pH = 6	92	0.33	[144]
NiO	*Solanum trilobatum*	Chlorophenol	UV light, 30 mg/L, pH = 9	92	4.17	[106]
NiO/g-C_3N_4	*Trinosphora cordifolia*	Tetracycline	Visible light (Xenon lamp), 0.2 g, 250 ml	98	1	[108]
NiO	*Trinosphora cordifolia*	Tetracycline	UV light, 0.25 g, 250 mL	99	0.5	[109]
NiO-ZnO	*Diospyros kaki*	4-nitrophenol	Sunlight, 10 ppm, 50 mL, 10 mg	70	0.75	[110]

Karthic et al. used *Araucacaria columaris*-synthesized NiO for the degradation of Carbamazepene and naproxen in municipal water bodies [142]. Efficiencies of 99% and 98% after 2.25 h was noted. When tested for their reusability and recyclability, the materials were reusable and the green NiO still maintained a defect-free pattern. A pseudo-first-order reaction was maintained with a rate constant of 2.6×10^{-2} for carbamazine and 2.5296×10^{-2} for naproxen. In this study (Figure 12), OH radicals were found to contribute to the direct destruction of pharmaceutical pollutants, as they target the bonds in the pharmaceuticals. From other studies, it was noted that factors such as particle size, structure, degradation route, oxidation, decarboxylation, and fragmentation play a role in how these NiO behave, and the mechanism of degradation is illustrated in Figure 12 [133,135].

Ezhillaris et al. used *Aegele marmelos*-mediated NiO for the degradation of 4-chlorophenol, an endocrine-disrupting pollutant [6]. At optimum conditions of pH 5 and 3.5 h, an 87% degradation of the pollutant was noted. Roopan et al., with Calotropis-mediated NiO and using sunlight and a shorter time period of degradation, noted a 94% efficiency for 4-nitrophenol [83]. Fatima et al., under UV–visible light and using a Xenon lamp, a green composite of NiO/rGo formed from *Pometia pinnata* showed an enhanced efficiency of 99% at 0.5 h [145]. The reduced crystallite size (42 nm) of the composite may have contributed to the improved degradation [106,143,146]. Pouthika et al. formed Cu-NiO-HT using *Carrisa edulis* [134]. In the presence of a 300 W Xenon lamp and after 1.5 h, 84% of the material was degraded [122,138]. Honarmand et al. (2022), using chitosan/cellulose NiO from barley and shrimp as reducing agents were also tested using sunlight for the

degradation of ciproflaxin [109]. A strong degradation of 92% in 30 min was observed. Lastly, Fatima et al. experienced a sharp degradation of 99% against tetracycline using NiO mediated with *Trinosphora cordifola* in less than 30 min [109]. From the LCMS analysis of the mechanism, a hydroxyl attacking the carbonyl was noted, and demethylation was observed. OHs and holes were recorded to be the species responsible for the high degradation. Moreover, they could be used at least five times with high efficiency.

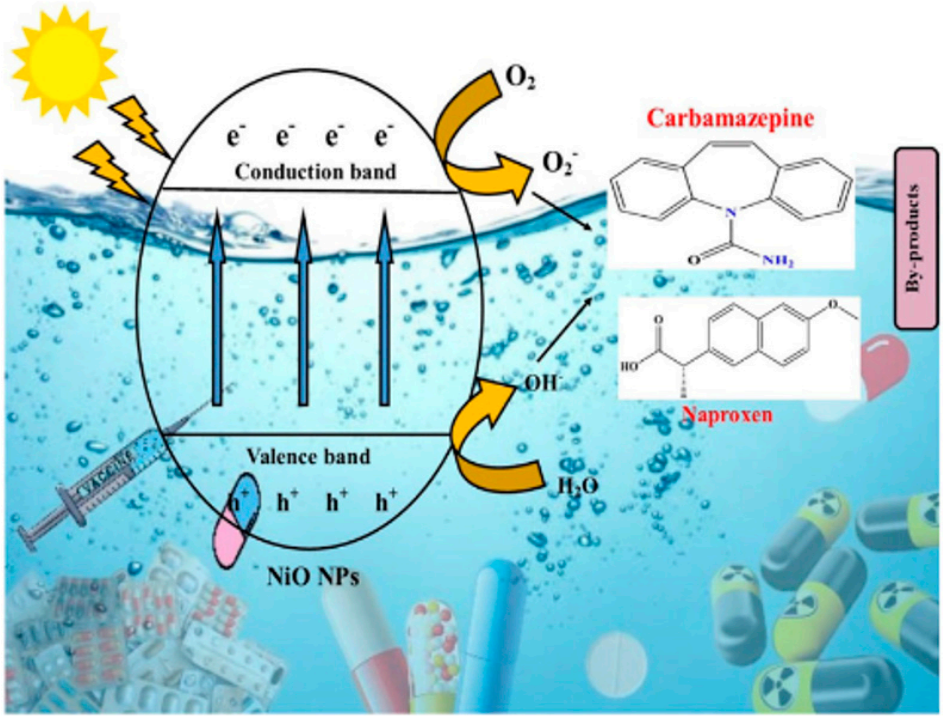

Figure 12. Green NiO for the degradation of Carbamazepene and naproxen [142].

From these studies, it can be noted that green NiO and its composites can serve as multifunctional materials for the degradation of dye colorants and pharmaceutical pollutants.

However, for the efficient usage of these green materials, factors such as the synthesis process, time constraints, extraction process, yield, and quality of the nanoparticles still hinder the usage of these materials in various applications, as well as the ability to be upscaled. For example, as to the quality of the nanoparticles synthesized using plant extracts, there is a high variability in terms of optical, morphological, and size properties. However, the conversion rate is not reported, as it has been shown that, based on the concentration, it can be minimal. Another concerning factor is the plant materials that are used for the synthesis. Some are only found in specific parts of the world or can only be produced during certain seasons. And other plants (*Arabica coffee*) take a long period (7 years) of time to be produced. Lastly, the biggest limitation is the synthesis process. First, most of the plants need to be preserved at temperatures below 4 °C. Several extraction steps need to be conducted, and the issue of high energy consumption (high reaction temperatures) is still being researched. Thus, until researchers are able to control the properties of these green materials and are able to engineer materials with good optical properties and specific surface areas, their application in the degradation and removal of various pollutants will still be limited.

7. Conclusions and Future Perspectives

The environmental impact of water contamination caused by the textile industry is substantial, with dye pollutants disrupting aquatic ecosystems, coloring the water, and reducing biodiversity.

To address the water contamination crisis, there is a need for various aspects involving stricter regulations, improved water treatment technologies, proper disposal by the textile industry, and public awareness campaigns. Investment in advanced filtration systems and real-time water quality monitoring can also significantly reduce the prevalence of these dye contaminants. The work that has been conducted in recent years through AOPs for dye degradation has been commendable, in particular regarding the environmentally friendly materials that have been produced. These materials are used as they also do not produce secondary pollutants. Though their synthesis has been greatly improved, they still suffer from limitations, such as low yield from production, uneven plant distribution, and still requiring long reaction times during synthesis. Thus, investigations and developments are still ongoing, not only on green synthesis but also on the modifications. Also, it is important to produce materials that do not only target one specific pollutant (dye) but various other pollutants (pharmaceuticals).

This review has shown that progress has been made in the synthesis of green modified materials, in particular the use of plant extracts. However, the highlighted limitations have been a barrier to the application of these materials as photocatalysts and their upscaling. As more studies progress, optimization studies should be more focused upon, and also, since it is known which type of compounds (enol and methyl) serve as reducing and capping agents, efficient extraction methods should be focused upon to assist in the synthesis of modified materials with suitable properties.

Author Contributions: Conceptualization, N.C.H.-M.; formal analysis and investigation, I.S., N.C.H.-M. and D.A.B.; writing—original draft preparation, I.S., D.A.B., L.M.M.-G., Z.T. and N.C.H.-M.; writing—review and editing Z.T., L.M.M.-G. and N.C.H.-M.; supervision and funding acquisition, N.C.H.-M. and D.A.B. All authors have read and agreed to the published version of the manuscript.

Funding: This research received no external funding.

Conflicts of Interest: The authors declare there is no conflict of interest.

References

1. Hamidian, K.; Rigi, H.; Najafidoust, A.; Sarani, M.; Miri, A. Study of the photocatalytic activity of green synthesized nickel oxide nanoparticles in the degradation of acid orange 7 dye under visible light. *Bioprocess Biosyst. Eng.* **2021**, *44*, 2667–2678. [CrossRef] [PubMed]
2. Robinson, D. What Causes Water Pollution and How Do We Solve It? 2022. Available online: https://earth.org/what-are-the-causes-of-water-pollution/ (accessed on 3 February 2025).
3. Oladoye, P.; Ajiboye, T.; Omotola, E.; Oyewola, O. Methylene blue dye: Toxicity and potential elimination technology from wastewater. *Results Eng.* **2022**, *16*, 100678. [CrossRef]
4. Al-Tohamy, R.; Ali, S.; Li, F.; Okasha, K.; Mahmound, Y.; Elsamahy, T.; Jiao, H.; Fu, Y.; Sun, J. A critical review on the treatment of dye-containing wastewater: Ecotoxicological and health concerns of textile dyes and possible remediation approaches for environmental safety. *Ecotoxicol. Environ. Saf.* **2022**, *231*, 113160. [CrossRef]
5. Shubha, J.P.; Savitha, H.S.; Patil, R.C.; Assal, M.E.; Shaik, M.; Kuniyil, M.; Alduhaish, O.; Dubasi, N.; Adil, S. A green approach for the degradation of toxic textile dyes by nickel oxide (NiO-SD) NPs: Photocatalytic and kinetic approach. *J. King Saud Univ. Sci.* **2023**, *35*, 102784. [CrossRef]
6. Ezhilarasi, A.A.; Vijaya, J.J.; Kaviyarasu, K.; Kennedy, L.J.; Ramalingam, R.J.; Al-Lohedan, H.A. Green synthesis of NiO nanoparticles using Aegle marmelos leaf extract for the evaluation of in-vitro cytotoxicity, antibacterial and photocatalytic properties. *J. Photochem. Photobiol. B Biol.* **2018**, *180*, 35–50. [CrossRef] [PubMed]

7. Yang, Y.; Wang, L.; Xiang, F.; Zhao, L.; Qiao, Z. Activated sludge microbial community and treatment performance of wastewater treatment plants in industrial municipal zones. *Int. J. Environ. Res. Public Health* **2020**, *17*, 436. [CrossRef]
8. Jiang, J.Q. The role of coagulation in water treatment. *Curr. Opin. Chem. Eng.* **2015**, *8*, 36–44. [CrossRef]
9. Ungureanu, N.; Vlăduț, V.; Cristea, M.; Cujbescu, D. Wastewater electrooxidation using stainless steel electrode. *E3S Web Conf.* **2020**, *180*, 10. [CrossRef]
10. Mishra, S.; Sundaram, B. A review of the photocatalytic process used for water waste treatment. *Mater. Today Proc.* **2023**, *102*, 393–409. [CrossRef]
11. Gared, R.M.; Kore, S.V.; Kore, V.S.; Kulkarni, G.S. A short review on process and application of reverse osmosis. *Univers. J. Environ. Res. Technol.* **2011**, *1*, 233–238.
12. Ren, G.; Han, H.; Wang, Y.; Liu, S.; Zhao, J.; Meng, X.; Li, Z. Recent Advances of Photocatalytic Application in Water Treatment: A Review. *Nanomaterials* **2021**, *11*, 1804. [CrossRef] [PubMed]
13. Hassaan, M.A.; El-Nemr, M.A.; Elkatory, M.R.; Ragab, S.; Niculescu, V.C.; El Nemr, A. Principles of Photocatalysts and their different applications: A Review. *Top. Curr. Chem.* **2023**, *381*, 31. [CrossRef]
14. Zhao, X.; Li, Z.; Yu, J.; Li, C.; Xu, S.; Li, F.; Zhang, C.; Man, B.; Zhang, C. Plasmonic and bi-piezoelectric enhanced photocatalysis using PVDF/ZnO/Au nanobrush. *Nanophotonics* **2022**, *11*, 3339–3349. [CrossRef]
15. Shi, M.; Qiu, T.; Tang, B.; Zhang, G.; Yao, R.; Xu, W.; Chen, J.; Fu, X.; Ning, H.; Peng, J. Temperature-Controlled Crystal Size of Wide Band Gap Nickel Oxide and Its Application in Electrochromism. *Macromachine* **2021**, *12*, 80. [CrossRef] [PubMed]
16. Hefnawy, M.A.; Fadlallah, S.A.; El-Sherif, R.M.; Medany, S.S. Synergistic effect of Cu-doped NiO for enhancing urea electrooxidation: Comparative electrochemical and DFT studies. *J. Alloys Compd.* **2021**, *896*, 162857. [CrossRef]
17. Karthik, K.; Shankshank, M.; Revathi, V.; Tarachuk, T. Facile microwave-assisted green synthesis of NiO nanoparticles from Andrographis paniculata leaf extract and evaluation of their photocatalytic and anticancer activities. *Mol. Cryst. Liq.* **2019**, *673*, 70–80. [CrossRef]
18. Dey, S.; Bhattacharjee, S.; Chaudhuri, M.G.; Bose, R.S.; Halder, S.; Ghosh, C.K. Synthesis of pure nickel(III) oxide nanoparticles at room temperature for Cr(VI) ion removal. *RSC Adv.* **2015**, *5*, 54717–54726. [CrossRef]
19. Rahdar, A.; Aliahmadb, M.; Azizib, Y. NiO Nanoparticles: Synthesis and Characterization. *J. Nanostruct.* **2015**, *5*, 145–151.
20. Zorkiplia, N.N.M.; Kausb, N.H.M.; Mohamada, A.A. Synthesis of NiO Nanoparticles through Sol-gel Method. *Procedia Chem.* **2016**, *19*, 626–631. [CrossRef]
21. Motene, K.; Mahlaule-Glory, L.M.; Ngoepe, M.N.; Mathipa, M.M. Photocatalytic degradation of dyes and removal of bacteria using biosynthesized flowerlike NiO nanoparticles. *Int. J. Environ. Anal. Chem.* **2023**, *103*, 1107–1122. [CrossRef]
22. Abid, N.; Khan, A.M.; Sujait, S.; Chaudhary, K.; Ikram, M.; Imran, M.; Haider, J.; Khan, M.; Khan, Q.; Maqbool, M. Synthesis of nanomaterials using various top down and bottom up approaches, influencing factors, advantages and disadvantages: A review. *Adv. Colloid Interface Sci.* **2022**, *300*, 102597. [CrossRef]
23. Tazikeh, S.; Akbari, A.; Talebi, A.; Talebi, E. Synthesis and characterization of tin oxide nanoparticles via the Co-precipitation method. *Mater. Sci. Pol.* **2014**, *32*, 99–101. [CrossRef]
24. Singh, P.; Kim, Y.; Zhang, D.; Yang, D. Biological Synthesis of Nanoparticles from Plants and Microorganisms. *Trends Biotechnol.* **2016**, *34*, 388–399. [CrossRef] [PubMed]
25. Li, J.; Wu, Q.; Wu, J. Synthesis of Nanoparticles via Solvothermal and Hydrothermal Methods. *Handb. Nanopart.* **2016**, 1–28. [CrossRef]
26. Madathil, A.N.P.; Vanaja, K.A.; Jayaraj, M.K. Synthesis of ZnO nanoparticles by hydrothermal method. *Nanophotonic Mater. IV* **2007**, *6639*, 47–55.
27. Langa, C.; Hintsho-Mbita, N.C. Plant and bacteria mediated synthesis on TiO_2 NPs for dye degradation in water. A review. *Chem. Phys. Impact* **2023**, *7*, 100293. [CrossRef]
28. Sabouri, Z.; Rangarazi, A.; Amiri, M.; Khatami, M.; Darroudi, M. Green synthesis of nickel oxide nanoparticles using *Salvia hispanica* L.(chia) seeds extract and studies of their photocatalytic activity and cytotoxicity effects. *Bioprocess Biosyst. Eng.* **2021**, *44*, 2407–2415. [CrossRef]
29. Álvarez-Chimal, R.; Arenas-Alatorre, J.Á. Green Synthesis of Nanoparticles: A Biological Approach. In *Green Chemistry for Environmental Sustainability Prevention-Assurance-Sustainability (P-A-S) Approach*; IntechOpen: London, UK, 2023. [CrossRef]
30. Hussain, I.; Singh, N.B.; Singh, A.; Singh, H.; Singh, S.C. Green synthesis of nanoparticles and its potential application. *Biotechnol. Lett.* **2015**, *38*, 545–560. [CrossRef]
31. Huston, M.; DeBella, M.; DiBella, M.; Gupta, A. Green Synthesis of Nanomaterials. *Nanomaterials* **2021**, *11*, 2130. [CrossRef]
32. Jadoun, S.; Arif, R.; Jangid, N.K.; Meena, R.K. Green synthesis of nanoparticles using plant extracts: A review. *Environ. Chem. Lett.* **2020**, *19*, 355–375. [CrossRef]
33. Kganyago, P.; Mahlaule-Glory, L.M.; Mathipa, M.M.; Ntsendwana, B.; Mketo, N.; Mbita, Z.; Hintsho-Mbita, N.C. Synthesis of NiO nanoparticles via a green route using Monsonia Burkeana; The Physical and Biological Properties. *J. Photochem. Photobiol. B Biol.* **2018**, *182*, 18–26. [CrossRef] [PubMed]

34. Ezhilarasi, A.A.; Vijaya, J.J.; Kaviyarasu, K.; Kennedy, L.J.; Maaza, M.; Ayeshamariam, A. Green synthesis of NiO nanoparticles using Moringa oleifera extract and their biomedical applications: Cytotoxicity effect of nanoparticles against HT-29 cancer cells. *J. Photochem. Photobiol. B Biol.* **2016**, *164*, 352–360. [CrossRef]
35. Hussain, S.; Muazzam, M.A.; Ahmed, M.; Ahmed, M.; Mustafa, Z.; Murtaza, S.; Ali, J.; Ibar, M.; Shahid, M.; Imran, M. Green synthesis of nickel oxide nanoparticles using Acacia nilotica leaf extracts and investigation of their electrochemical and biological properties. *J. Taibah Univ. Sci.* **2023**, *17*, 2170162. [CrossRef]
36. Kundu, M.; Karunakaran, G.; Kuznetsov, D. Green synthesis of NiO nanostructured materials using *Hydrangea paniculata* flower extracts and their efficient application as supercapacitor electrodes. *Powder Technol.* **2017**, *311*, 132–136. [CrossRef]
37. Din, S.U.; Iqbal, H.; Haq, S.; Ahmad, P.; Khandaker, M.U.; Elansary, H.O.; Al-Harbi, F.F.; Abdelmohsen, S.A.M.; El-Abedin, T.K.Z. Investigation of the Biological applications of Biosynthesizes Nickel Oxide nanoparticles mediated by Buxus wallichiana extract. *Crystals* **2022**, *12*, 146. [CrossRef]
38. Reddy, V.L.; Lakshmikanth, S. Synthesis of NiO nanoparticles prepared via a green process using *Azadirachta indica*, *Morinda citrifolia*, and *Terminalia elliptica* for biological applications. *BioNanoScience* **2023**, *13*, 1184–1196. [CrossRef]
39. Saleem, S.; Ahmed, B.; Khan, M.S.; Al-Shaeri, M.; Musarrat, J. Inhibition of growth and biofilm formation of clinical bacterial isolates by NiO nanoparticles synthesized from Eucalyptus globulus plants. *Microb. Pathog.* **2017**, *111*, 375–387. [CrossRef]
40. Bekele, H.A.; Mohammed, O. Plant Extract Mediated Synthesis of Nickel Oxide nanoparticles. *Mater. Int.* **2020**, *2*, 0205–0209.
41. Sabouri, Z.; Akbari, A.; Hosseini, H.A.; Khatami, M.; Darroudi, M. Green-based biosynthesis of nickel oxide nanoparticles in Arabic gum and examination of their cytotoxicity, photocatalytic and antibacterial effects. *Green Chem. Lett. Rev.* **2021**, *14*, 404–414. [CrossRef]
42. Uddin, S.; Safdar, L.B.; Anwar, S.; Iqbal, J.; Laila, S.; Abbasi, B.A.; Saif, M.S.; Ali, M.; Rehman, A.; Basit, A.; et al. Green Synthesis of Nickel Oxide Nanoparticles from Berberis balochistanica Stem for Investigating Bioactivities. *Molecules* **2021**, *26*, 1548. [CrossRef]
43. Gebretinsae, H.G.; Tsegay, M.G.; Nuru, Z.Y. Biosynthesis of nickel oxide (NiO) nanoparticles from cactus plant extract. *Mater. Today Proc.* **2021**, *36*, 566–570. [CrossRef]
44. Feiona, T.A.; Sabeena, G.; Bagavathy, M.S.; Pushpalaksmi, E.; Samraj, J.J.; Annadurai, G. Recent Advances in the Synthesis and Characterization of Nanoparticles: A Green Adeptness for Photocatalytic and Antibacterial Activity. *Nat. Environ. Pollut. Technol.* **2021**, *20*, 657–663. [CrossRef]
45. Iqbal, J.; Abbasi, B.A.; Ahmad, R.; Mahmoodi, M.; Munir, A.; Zahra, S.A.; Shahbaz, A.; Shaukat, M.; Kanwal, S.; Uddin, S.; et al. Phytogenic Synthesis of Nickel Oxide Nanoparticles (NiO) Using Fresh Leaves Extracts of *Rhamnus trietra* (Wall) and Investigation of its Multiple In Vitro. *Biomedicines* **2020**, *8*, 117. [CrossRef]
46. Haides, A.; Ijaz, M.; Ali, S.; Haider, J.; Imran, M.; Majeed, H.; Shahzadi, I.; Ali, M.M.; Khan, J.A.; Ikram, M. Green Synthesized Phytochemically (*Zingiber officinale* and *Allium sativum*) Reduced Nickel Oxide Nanoparticles Confirmed Bactericidal and Catalytic Potential. *Nanoscale Res. Letters* **2020**, *15*, 50.
47. Khan, S.A.; Shahid, S.; Ayaz, A.; Alkahtani, J.; Elshikh, M.S.; Riaz, T. Phytomolecules-Coated NiO Nanoparticles Synthesis Using Abutilon indicum Leaf Extract: Antioxidant, Antibacterial, and Anticancer Activities. *Int. J. Nanomed.* **2021**, *16*, 1757–1773. [CrossRef] [PubMed]
48. Shwetha, C.R.; Kumar, R.; Kiran, C.R.; Betageri, V.S.; Latha, M.S.; Veerapur, R.; Lamroui, G.; Al-Kheraif, A.A.; Elgorban, A.M.; Syed, A.; et al. Biogenic Sythesis of NiO Nanoparticles Using Areca catechu Leaf Extract and Their Antidiabetic and cytotoxic Effects. *Molecules* **2021**, *26*, 2448.
49. Zhang, Y.; Mahdavi, B.; Mohammadhosseini, M.; Rezaei-Seresht, E.; Paydarfard, S.; Qorbani, M.; Karimain, M.; Abbasi, N.; Ghaneialvar, H.; Karimi, E. Green synthesis of NiO nanoparticles using Calendula officinalis extract: Chemical characterization, antioxidant, cytotoxicity, and anti-esophageal carcinoma properties. *Arab. J. Chem.* **2021**, *14*, 103105. [CrossRef]
50. Noukelag, S.K.; Mohamed, H.E.A.; Moussa, B.; Razanamahandry, L.C.; Ntwampe, S.K.O.; Arendse, C.J. Structural and optical investigations of biosynthesized bunsenite NiO nanoparticles (NPs) via an aqueous extract of *Rosmarinus officinalis* (rosemary) leaves. *Mater. Today Proc.* **2021**, *36*, 245–250. [CrossRef]
51. Haq, S.; Dildar, S.; Ali, M.B.; Maznr, A.; Hedfi, A.; Shahzad, M.I.; Shazad, N.; Shah, A. Antimicrobial and antioxidant properties of biosynthesized of NiO nanoparticles using *Raphanus sativus* (*R. sativus*) extract. *Mater. Res. Express* **2021**, *8*, 055006. [CrossRef]
52. Zhang, Q.; Xu, S.; Li, Y.; Ding, P.; Zhang, Y.; Zhao, P. Green-synthesized nickel oxide nanoparticles enhances biohydrogen production of *Klebsialla* sp. WL 1316 using lignocellulosic hydrolysate and its regulatory mechanism. *Fuel* **2021**, *305*, 121585. [CrossRef]
53. Priya, A.; Saminathan, S.; Balasundaran, J. Green synthesis of NiO nanoparticles using Leucas Aspera and its antibacterial activity. *Little Appl. NanoBioSci.* **2020**, *9*, 1033–1036.
54. Kumar, M.S.S.; Soundarya, T.L.; Nagaraju, G.; Raghu, G.K.; Rekha, N.D.; Alharthi, F.A.; Nirmala, B. Multifunctional applications of nickel oxide (NiO) nanoparticles synthesized by facile green combustion method using *Limonia acidissima* natural fruit juice. *Inorganica Chim. Acta* **2021**, *515*, 120059. [CrossRef]

55. Srihasam, S.; Thyagarajan, K.; Korivi, M.; Lebaka, V.R.; Mallem, S.P.R. Phytogenis generation of NiO nanoparticles using *Stevia leaf* extract and evaluation of their in-vitro antioxidant and antimicrobial properties. *Biomolecules* **2020**, *10*, 89. [CrossRef]
56. Ramesh, R.; Yamini, V.; Sundaram, S.J.; Khan, F.L.A.; Kaviyarasu, K. Investigation of structural and optical properties of NiO nanoparticles mediated by *Plectranthus amboinicus* leaf extract. *Mater. Today Proc.* **2021**, *36*, 268–272. [CrossRef]
57. Boudaif, M.; Messai, Y.; Bentouhami, E.; Schmutz, M.; Blanck, C.; Ruhlmann, L.; Bezzi, H.; Tairi, L.; Mekki, D.E. Green synthesis of NiO nanopaerticles using *Nigella sativa* extract and their enhanced electro-catalytic activity for the 4-nitrophenol degradation. *J. Phys. Chem. Solids* **2021**, *153*, 110020. [CrossRef]
58. Iqbal, A.; Haq, A.U.; Cerrón-Calle, G.A.; Naqvi, S.A.R.; Westerhoff, P.; Garcia-Segura, S. Green Synthesis of Flower-Shaped Copper Oxide and Nickel Oxide Nanoparticles Via Capparis Decidua Leaf Extract for synergic Adsorption-Photolytic Degradation of Pesticides. *Catalysts* **2021**, *11*, 806. [CrossRef]
59. Sheikh-Mohseni, M.H.; Sedaghat, S.; Derakhshi, P.; Safekordi, A. Green biosynthesis of Ni/montmorillonite nanoparticles using extract of Allium Jesdianum as the nano-catalyst for electrocatalytic oxidation of methanol. *Chin. J. Chem. Eng.* **2020**, *28*, 2555–2565. [CrossRef]
60. Mandal, B.K.; Mandal, R.; Sikdar, S.; Sarma, S.; Srinivasan, A.; Chowdhury, S.R.; Das, B.; Das, R. Green synthesis of NiO nanoparticle using *Punica granatum* peel extract and its characterization for methyl orange degradation. *Mater. Today Commun.* **2023**, *34*, 105302. [CrossRef]
61. Prabhu, S.; Thangadurai, T.D.; Bharathy, P.V.; Kalugasalam, P. Synthesis and characterization of nickel oxide nanoparticles using Clitoria Ternatea flower extract: Photocalytic dye degradation under sunlight and antibacterial activity applications. *Results Chem.* **2022**, *4*, 100285. [CrossRef]
62. Chouke, P.B.; Potbhare, A.K.; Meshram, N.P.; Rai, M.M.; Dadure, K.M.; Chaudhary, K.; Rai, A.R.; Desimone, M.F.; Chaudhary, R.G.; Masram, D.T. Bioinspired NiO Nanospheres: Exploring In Vitro Toxicity usimg Bm-17 and *L. rohita* Liver cells, DNA degradation, docking and proposed vacuolization mechanism. *Acs Omega* **2022**, *7*, 6869–6884. [CrossRef] [PubMed]
63. Nazaripour, E.; Mosazadeh, F.; Rahimi, S.S.; Alijani, H.Q.; Isaei, E.; Borhani, F.; Iravani, S.; Ghasemi, M.; Akbarizadeh, M.R.; Azizi, E.; et al. Ferromagnetic nickel oxide nanoparticles: Biosynthesis, characterization and their antibacterial activities. *Randiconti Lincei Sci. Fis. E Nat.* **2022**, *33*, 127–134. [CrossRef]
64. Baytar, O.; Ekinci, A.; Şahin, S.; Kutluay, S. Green synthesis of NiO from watermelon seed shell extract for the evaluation of H_2 production from $NaBH_4$ hydrolysis and photocatalytic reduction of methylene blue. *Mater. Sci. Eng. B* **2023**, *296*, 116704. [CrossRef]
65. Mathekga, K.; Hintsho-Mbita, N.C. Synthesis of *C. Benghanlensis* NiO NPs for the degradation of malachite green and the removal of bacteria. *Chem. Phys. Impact* **2023**, *7*, 100277. [CrossRef]
66. Singh, G.P.; Singh, K.J.; Chandel, K.; Kaur, P.; Kaur, J. Green synthesis of NiO doped CuO nanoparticles: Potential for environmental remediation. *Inorg. Chem. Commun.* **2023**, *157*, 111250. [CrossRef]
67. Ahmad, W.; Kaur, N. Microwave-assisted single step green synthesis of NiO nanoparticles using *Coleus scutellariodes* leaf extract for photolytic degradation of refloxacin. *MRS Adv.* **2023**, *8*, 835–842. [CrossRef]
68. Bhoye, M.; Pansambal, S.; Basnet, P.; Lin, K.A.; Gutierrez, K.Y.; Pérez, A.; Chauhan, A.; Oza, R.; Ghotekar, S. Eco-friendly synthesis of Ni/NiO nanoparticles using *Gymnema sylvestre* leaves extracts for antifungal activity. *J. Compos. Sci.* **2023**, *7*, 105. [CrossRef]
69. Anitha, S.; Balu, A.R.; Balamurugan, S.; Suganya, M.; Delci, Z.; Karthika, M.; Kayathiri, C.; Devi, S.C. A comparative study on the photocatalytic performance of two third order NLO active nanocomposites (NiO-Cd0 and NiO-CuO) green synthesized using *Psidium guajava* leaf extract. *Inorg. Chem. Commun.* **2021**, *134*, 109073. [CrossRef]
70. Din, M.I.; Nabi, A.G.; Rani, A.; Aihetasham, A.; Mukhtar, M. Single step green synthesis of stable nickel and nickel oxide nanoparticles from *Calotropis gigantea*: Catalytic and antimicrobial potentials. *Environ. Nanotechnol. Monit. Manag.* **2018**, *9*, 29–36. [CrossRef]
71. Ahmad, B.; Khan, M.I.; Naeem, M.A.; Alhodaib, A.; Fatima, M.; Amami, M.; Al-Abbad, E.A.; Kausar, A.; Alwadai, N.; Nazir, A.; et al. Green synthesis of NiO nanoparticles using *Aloe vera* gel extract and evaluation of antimicrobial activity. *Mater. Chem. Phys.* **2022**, *288*, 126363. [CrossRef]
72. Ciqueira, C.; Schons, A.B.; Appelt, P.; Silva, W.D.; Balaba, N.; Cunha, M.; Anaissi, F. Synthesis of green Brucite by incorporation of nickel ions in the periclase phase (MgO) applied as pigments. *Colorants* **2024**, *3*, 138–151. [CrossRef]
73. Neto, V.O.S.; de Castro, A.J.R.; Saraiva, G.D.; do Nascimento, R.F. Nanomaterials for groundwater remediation. *Compr. Anal. Chem.* **2022**, *99*, 135–162.
74. Behera, A.; Mittu, B.; Padhi, S.; Patra, N.; Singh, J. Chapter 25—Bimetallic nanoparticles: Green synthesis, applications, and future perspectives. In *Multifunctional Hybrid Nanomaterials for Sustainable Agri-Food and Ecosystems*; Elsevier: Amsterdam, The Netherlands, 2022; pp. 639–682.
75. Gebre, S.H. Bio-inspired synthesis of metal and metal oxide nanoparticles: The key role of phytochemicals. *J. Clust. Sci.* **2022**, *34*, 665–704. [CrossRef]

76. Sabouri, Z.; Fereydouni, N.; Akbari, A.; Hosseini, H.A.; Hashemzadeh, A.; Amiri, M.S.; Oskuee, R.K.; Darroudi, M. Plant-Based synthesis of NiO nanoparticles using salvia macrosiphon Boiss extract and examination of their water treatment. *Rare Matels* **2019**, *39*, 1134–1144. [CrossRef]
77. Sone, B.T.; Manikandan, E.; Gurib-Fakim, A.; Maaza, M. Sm2O3 nanoparticles green synthesis via *Callistemon viminalis*' extract. *J. Alloys Compd.* **2015**, *650*, 357–362. [CrossRef]
78. Din, M.I.; Rani, A. Recent advances in the synthesis and stabilization of nickel and nickel oxide nanoparticles: A green adeptness. *Int. J. Anal. Chem.* **2016**, *2016*, 3512145.
79. Nallathambi, D.; Sangeeth, R.; Geethapriya, J.; Nagoormeeran, M. Green fabriacated NiO spherical nanoparticles for photocatalytic assays of textile dye degradation. *J. Indian Chem. Soc.*. [CrossRef]
80. Diao, C.C.; Huang, C.Y.; Chen, C.Y.; Wu, C.C. Morphological, optical and electrical properties of p-type nickel oxide thin films by nonvacuum deposition. *Nanomaterials* **2020**, *10*, 636. [CrossRef]
81. Laid, D.; Zaouche, C.; Yamina, B.; Abdelouahab, G. Structural properties of nanostructured NiO thin films prepared by spray pyrolysis technique. *Tob. Regul. Sci.* **2023**, *9*, 2819–2831.
82. Al-Zaqri, N.; Umamakeshvari, K.; Mohana, V.; Muthuvel, A.; Boshaala, A. Green synthesis of nickel oxide nanoparticles and its photocatalytic degradation and antibacterial activity. *J. Mater. Sci. Mater. Electron.* **2022**, *33*, 11864–11880. [CrossRef]
83. Roopan, S.M.; Elango, G.; Priya, D.D.; Asharani, I.V.; Kishore, B.; Vinayprabhakar, S.; Pragatheshwaran, N.; Mohanraj, K.; Harshpriya, R.; Shanavas, S.; et al. Sunlight mediated photocatalytic degradation of organic pollutants by statistical optimization of green synthesized NiO NPs as catalyst. *J. Mol. Liq.* **2019**, *293*, 111509. [CrossRef]
84. Din, M.I.; Tariq, M.; Hussain, Z.; Khalid, R. Single step green synthesis of nickel and nickel oxide nanoparticles from *Hordeum vulgare* for photocatalytic degradation of methylene blue dye. *Inorg. Nano-Met. Chem.* **2020**, *50*, 292–297. [CrossRef]
85. Rafique, M.A.; Kiran, S.; Javed, S.; Ahmad, I.; Yousaf, S.; Iqbal, N.; Afzal, G.; Rani, F. Green synthesis of nickel oxide nanoparticles using *Allium cepa* peels for degradation of Congo red direct dye: An environmental remedial approach. *Water Sci. Technol.* **2021**, *84*, 2793–2804. [CrossRef] [PubMed]
86. Hamdan, A.; Sardi, A.; Reksamunandar, R.P.; Maulida, Z.; Arsa, D.A.; Lubis, S.S.; Nisah, K. Green synthesis of NiO using a hyperacumulator (*Lactucal Savita* L.) and its application as Pb (II) and Cu (II) adsorbent. *Environ. Nanotechnol. Monit. Manag.* **2024**, *21*, 100910.
87. Barzinjy, A.A.; Hamad, S.M.; Aydın, S.; Ahmed, M.H.; Hussain, F.H.S. Green and eco-friendly synthesis of Nickel oxide nanoparticles and its photocatalytic activity for methyl orange degradation. *J. Mater. Sci. Mater. Electron.* **2020**, *31*, 11303–11316. [CrossRef]
88. Khan, Z.U.H.; Khan, A.; Shah, N.S.; Din, I.U.; Salam, M.A.; Iqbal, J.; Muhammad, N.; Imran, M.; Ali, M.; Sayed, M.; et al. Photocatalytic and biomedical investigation of green synthesized NiO NPs: Toxicities and degradation pathways of Congo red dye. *Surf. Interfaces* **2021**, *23*, 100944. [CrossRef]
89. Lema Gemachu, Y.; Birhanu, A.L. Green synthesis of ZnO, CuO and NiO nanoparticles using Neem leaf extract and comparing their photocatalytic activity under solar irradiation. *Green Chem. Lett. Rev.* **2024**, *17*, 2293841. [CrossRef]
90. Meena, J.; Dinakaran, A.; Kumaraguru, N.; Veerappa, N.S.; Shin, P.K.; Tatsugi, J.; Kumar, A.; Santhakumar, A.; Thangadurai, T.D.; Bharathy, P.V.; et al. Bioengineered NiO nanofabrication for energy storage systems, degradation of refractory water toxicity and antibacterial study. *Chem. Sel.* **2024**, *9*, e202402521.
91. Jeba, D.P.; Amaladhas, T.P. Green synthesis and photocatalytic activity of nickel oxide nanostructures in the degradation of organic dyes. *Int. J. Res. Advert Technol.* **2018**, *6*, 2321–9637.
92. Sabouri, Z.; Akbari, A.; Hosseini, H.A.; Khatami, M.; Darroudi, M. Tragacanth-mediate synthesis of NiO nanosheets for cytotoxicity and photocatalytic degradation of organic dyes. *Bioprocess Biosyst. Eng.* **2020**, *43*, 1209–1218. [CrossRef] [PubMed]
93. Ghmari, E.B.; Farah, H.; Ech-Chahad, A. Biosynthesis, Characterization of Nickel(II) Oxide Nanoparticles NiO and their High-Efficient Photocatalytic Application. *Int. J. Nanosci. Nanotechnol.* **2023**, *19*, 135–147.
94. Legmairi, S.; Meneceur, S.; Bouafia, A.; Laouini, S.E.; Alshareef, S.A.; Al-Essa, K.; Almukhlifi, H.A.; Tedjani, M.L.; Menaa, F. Biofabrication of NiO and NiO-decorated Fe nanocomposite efficiency for removal of methylene blue from aqueous solution. *Biomass Convers. Biorefin.* **2023**, *14*, 18469–18479. [CrossRef]
95. Ravichandran, S.; Sengodan, P.; Radhakrishnan, J. Evaluation of biosynthesized nickel oxide nanoparticles from *Clerodendrum phlomidis*: A promising photocatalyst for methylene blue and acid blue dyes degradation. *Ceram. Int.* **2023**, *49*, 12408–12414. [CrossRef]
96. Jagan, K.S.G.; Surendhiran, S.; Savitha, S.; Balu, K.S.; Karthik, A. Distinct nickel-precursor synthesized NiO NPs on the degradation of biological staining dyes: A green route. *J. Mater. Sci. Mater. Electron.* **2024**, *35*, 169. [CrossRef]
97. Ghazal, S.; Akbari, A.; Hosseini, H.A.; Sabouri, Z.; Forouzanfar, F.; Khatami, M.; Darroudi, M. Sol-gel biosynthesis of nickel oxide nanoparticles using *Cydonia oblonga* extract and evaluation of their cytotoxicity and photocatalytic activities. *J. Mol. Struct.* **2020**, *1217*, 128378. [CrossRef]

98. Puttaraju, T.D.; Soundarya, T.L.; Nagaraju, G.; Lingaraju, K.; Manjula, M.V.; Devaraja, S.; Manjunatha, M. Biogenic approach for synthesis of ZnO/NiO nanocomposites as a highly efficient photocatalyst and evaluation of their biological properties. *Braz. J. Chem. Eng.* **2023**, 1–14. [CrossRef]
99. Sundaresan, N.; Ravichandran, S. Biosynthesis of nickel oxide nanoparticles using *Evolvulus alsinoides* extract and their potential photocatalytic and invitro anticancer activity. *Inorg. Chem. Commun.* **2023**, *150*, 110489. [CrossRef]
100. Singh, A.; Goyal, V.; Singh, J.; Kaur, H.; Kumar, S.; Batoo, K.M.; Gaur, J.; Pal, M.; Rawat, M.; Hussain, S. Structurally and morphologically engineered single-pot biogenic synthesis of NiO nanoparticles with enhanced photocatalytic and antimicrobial activities. *J. Clean. Prod.* **2022**, *343*, 131026. [CrossRef]
101. Singh, V.; Sapehia, R.; Dhiman, V. Removal of methylene blue dye by green synthesized NiO/ZnO nanocomposites. *Inorg. Chem. Commun.* **2024**, *162*, 112267. [CrossRef]
102. Blizak, D.; Remli, S.; Blizak, S.; Bouchenak, O.; Yahiaoui, K. NiO thin films for environmental photocatalytic applications: A review. *Alger. J. Environ. Sci. Technol.* **2021**, *7*, 1950–1957.
103. Ramesh, M. N and Fe doped NiO nanoparticles for enhanced photocatalytic degradation of azo dye methylene blue in the presence of visible light. *SN Appl. Sci.* **2021**, *3*, 817. [CrossRef]
104. Hussein, B.Y.; Mohammed, A.M. Biosynthesis and characterization of nickel oxide nanoparticles by using aqueous grape extract and evaluation of their biological applications. *Results Chem.* **2021**, *3*, 100142. [CrossRef]
105. Mayedwa, N.; Mongwaketsi, N.; Khamlich, S.; Kaviyarasu, K.; Matinise, N.; Madza, M. Green synthesis of nickel oxide, palladium and palladium oxide synthesized via *Aspalathus linearis* natural extracts: Physical properties and mechanism of formation. *Appl. Surf. Sci.* **2017**, *446*, 266–272. [CrossRef]
106. Ezhilarasi, A.A.; Vijaya, J.J.; Kaviyarasu, K.; Zhang, X.; Kennedy, L.J. Green synthesis of nickel oxide nanoparticles using *Solanum trilobatum* cytotoxicity, antibacterial and photocatalytic studies. *Surf. Interfaces* **2020**, *20*, 100553. [CrossRef]
107. Rani, M.; Rishab; Kaur, D.; Shanker, U.; Sillanpaa, M. Green synthesized N-CQDs@NiO nanocomposites for efficient photocatalytic degradation of organic pollutants from water. *Inorg. Chem. Commun.* **2024**, *2*, 113326. [CrossRef]
108. Fatimah, I.; Sulistyowati, R.Z.; Wijayana, A.; Purwiandono, G.; Sagadevan, S. Z-scheme NiO/g-C3N4 nanocomposites prepared using phyto-mediated nickel nanoparticles for the efficient photocatalytic degradation. *Heliyon* **2023**, *9*, e16232. [CrossRef]
109. Fatimah, I.; Wijayana, A.; Ramanda, G.D.; Sagadevan, S.; Oh, W.C.; Doong, R. Highly active photocatalyst of nickel oxide nanoparticles green synthesized using Trinosphora cordifolia-plant extract for photocatalytic oxidation of tetracycline. *Environ. Nanotechnol. Monit. Manag.* **2024**, *22*, 100968.
110. Haq, S.; Raja, A.W.; Rehman, S.U.; Mezni, A.; Ali, M.B.; Hedfi, A.; Shahzad, M.I.; Rehman, W.; Shahzad, N.; Waseem, M.; et al. Phytogenic synthesis and characterization of NiO-ZnO nanocomposite for the photodegradation of Brilliant Green and 4-Nitrophenol. *J. Chem.* **2021**, 3475036. [CrossRef]
111. Louafi, O.; Khelef, A.; Zeroual, S.; Laouini, S.E.; Tedjani, M.L. Efect of Nickel Nitrate Concentration on the Size of Nickel Oxide Nanoparticles Bio-synthesized by Artemisia herba-alba Aqueous Leaves Extract and Improving Their Antioxidant Activities. *J. Inorg. Organomet. Polym. Mater.* **2022**, *32*, 1116–1128. [CrossRef]
112. Rawool, S.A.; Pai, M.R.; Banerjee, A.M.; Arya, A.; Ningthoujam, R.S.; Tewari, R.; Rao, R.; Chalke, B.; Ayyub, P.; Tripathi, A.K.; et al. pn Heterojunctions in NiO: TiO_2 composites with type-II band alignment assisting sunlight driven photocatalytic H_2 generation. *Appl. Catal. B Environ.* **2018**, *221*, 443–458. [CrossRef]
113. Villamayor, A.; Pomone, T.; Perero, S.; Ferraris, M.; Barrio, V.L.; Eva, G.; Kelly, P. Development of photocatalytic nanostructured TiO_2 and NiO/TiO_2 coatings by DC magnetron sputtering for photocatalytic applications. *Ceram. Int.* **2023**, *49*, 19309–19317. [CrossRef]
114. Ramesh, M.; Rao, M.P.C.; Anandan, S.; Nagaraja, H. Adsorption and photocatalytic properties of NiO nanoparticles synthesized via a thermal decomposition process. *J. Mater. Res.* **2018**, *33*, 601–610. [CrossRef]
115. Aminuzzaman, M.; Chong, C.; Goh, W.; Phang, Y.; Lai-Hock, T.; Chee, S.; Akhtaruzzaman, M.; Ogawa, S.; Watanabe, A. Biosynthesis of NiO nanoparticles using soursop (*Annona muricata* L.) fruit peel green waste and their photocatalytic performance on crystal violet dye. *J. Clust. Sci.* **2021**, *32*, 949–958. [CrossRef]
116. Subashini, K.; Prakash, S.; Devi, V.S.A.; Sujatha, V. Dye degradation efficiency of green synthesized NiO @ GO nanocomposite with biological application. *J. Phys. Conf. Ser.* **2022**, *2225*, 012005. [CrossRef]
117. Kannan, K.; Radhika, D.; Nikolova, M.P.; Sadasivuni, K.K.; Mahdizadeh, H.; Verma, M. Structural studies of bio-mediated NiO nanoparticles for photocatalytic and antibacterial activities. *Inorg. Chem. Commun.* **2020**, *113*, 107755. [CrossRef]
118. Yadav, S.; Tiwari, K.S.; Gupta, C.; Tiwari, M.K.; Khan, A.; Sonkar, S.P. A brief overview of natural dyes, pigments: Recent Advances and Future Perspectives. *Results Chem.* **2023**, *5*, 100733. [CrossRef]
119. Kalita, C.; Sarma, N.; Sarkar, R.D.; Hoque, S.; Das, M.R.; Saikia, P. Facile synthesis of Cu-Ni bimetallic nanoparticles using peppermint leaf extract for enhanced antimicrobial efficacy and solar-driven photocatalytic activity. *Emergent Mater.* **2023**, *7*, 221–233. [CrossRef]
120. Wang, Z.; Yue, X.; Xiang, Q. MOFs-Based S-scheme heterojunction photocatalyst. *Coord. Chem. Rev.* **2024**, *504*, 215674. [CrossRef]

121. Swetha, S.; Janani, B.; Khan, S.S. A critical review on the development of metal-organic frameworks for boosting photocatalysis in the fields of energy and environment. *J. Clean.* **2021**, *333*, 130164. [CrossRef]
122. Boonserm, K.; Sutcha, A.; Phinjaroenphan, R. Green synthesis of bimetallic CuO@NiO nanocomposite for the removal of glyphosate. *J. Met. Mater. Miner.* **2024**, *34*, 1931. [CrossRef]
123. Ju, Y.; Wang, Z.; Lin, H.; Hou, R.; Li, H.; Wang, Z.; Zhi, R.; Lu, X.; Tang, Y.; Chen, F. Modulating the microenvironment of catalytic interface with functional groups for efficient photocatalytic degradation of persistent organic pollutants. *Chem. Eng. J.* **2023**, *479*, 147800. [CrossRef]
124. Bavaji, S.R.; Ahamed, A.J. Synthesis of Cu doped NiO for their antioxidant and photocatalytic properties: Green synthesis using Lycopodium Linn. *Chem. Phys. Impact* **2024**, *8*, 100647. [CrossRef]
125. Firisa, S.G.; Muleta, G.G.; Yimer, A.A. Synthesis of nickel oxide nanoparticles and copper-doped nickel oxide nanocomposites using *Phytolacca dodecandra* L'Herit leaf exact and evaluation of its antioxidant and photocatalytic activities. *ACS Omega* **2022**, *7*, 44720–44732. [CrossRef]
126. Kanwal, A.; Shahzadi, T.; Riaz, T.; Zaib, M.; Khan, S.; Habila, M.A.; Sillanpaa, M. Photocatalytic degradation studies of organic dyes over novel Cu/Ni loaded reduced graphene oxide hybrid nanocomposite: Adsorption, kinetics and thermodynamics studies. *Molecules* **2023**, *28*, 64–74. [CrossRef] [PubMed]
127. Ismail, M.; Khan, M.I.; Khan, S.B.; Khan, M.A.; Akhtar, K.; Asiri, A.M. Green synthesis of plant supported Cu-Ag and Cu-Ni bimetallic nanoparticles in the reaction of nitrophenols and organic dyes for water treatment. *J. Mol. Liq.* **2018**, *260*, 78–91. [CrossRef]
128. Prabhu, S.; Thangadurai, T.D.; Indumathi, T.; Kalugasalam, P. Enhanced visible light induced dye degradation and antibacterial activities of ZnO/NiO nanocomposites synthesized using *Clitoria ternatea* flower extract flower extract. *Inorg. Chem. Commun.* **2022**, *146*, 110077. [CrossRef]
129. Weng, X.; Guo, M.; Luo, F.; Chen, Z. One-step green synthesis of bimetallic Fe/Ni nanoparticles of eucalyptus leaf extract: Biomolecules identification, characterization and catalytic activity. *Chem. Eng. J.* **2017**, *308*, 904–911. [CrossRef]
130. Mohan, S.; Devan, M.V. Photocatalytic activity of Ag/Ni bi-metallic nanoparticles on textile dye removal. *Green Process. Synth.* **2019**, *8*, 895–900. [CrossRef]
131. Foster, S.L.; Estoque, K.; Voecks, M.; Rentz, N.; Greenlee, L.F. Removal of synthetic Azo dye using bimetallic Nickel-Iron nanoparticles. *J. Nanomater.* **2019**, *2019*, 9807605. [CrossRef]
132. Tang, M.; Snoussi, Y.; Bhakta, A.K.; Garah, M.E.; Khalil, A.M.; Ammar, S.; Chehimi, M.M. Unusual hierarchically structured composite of sugarcane pulp bagasse biochar loaded with Cu/Ni bimetallic nanoparticles for dye removal. *Environ. Res.* **2023**, *232*, 116232. [CrossRef] [PubMed]
133. Shakila, P.B.; Jeevanantham, V.; Nagalakshmi, R.; Saravanan, R. Quick photoresponsive and high quantum yield of Ag/Pd/Ni trimetallic nanocatalyst using *Cassia auriculata* for removal of fabric dye. *Biomass Convers. Biorefin.* **2023**, *14*, 25533–25543. [CrossRef]
134. Pouthika, K.; Madhumitha, G. Design and development of *Carissa edulis* fruit extract mediated bimetallic CuO-NiO-HNT composites for photocatalytic removal of food dye and antibiotic dye. *J. Mol. Struct.* **2024**, *1295*, 136665. [CrossRef]
135. Huang, X.; Zafar, A.; Ahmad, K.; Hasan, M.; Tariq, T.; Gong, S.; Hassan, S.G.; Guo, J.; Javed, H.U.; Shu, X. Biological synthesis of bimetallic hybrid nanocomposite: A remarkable photocatalyst, adsorption/desorption and antimicrobial agent. *Appl. Surf. Sci. Adv.* **2023**, *17*, 100446. [CrossRef]
136. Haque, B.; Gupta, A.; Roy, A.; Malik, A.; Khan, A.A. Green fabrication of Ag-Ni-Mn-Zn nanoparticles from watermelon peels and its antioxidants, dye degradation ang molecular docking studies. *Clean Technol. Environ. Policy* **2024**, 1–28.
137. Mahlaule-Glory, L.M.; Mathobela, S.; Hintsho-Mbita, N.C. Biosynthesized bimetallic ($ZnOSnO_2$) nanoparticles for photocatalytic degradation of organic dyes and pharmaceutical pollutants. *Catalysts* **2022**, *12*, 334. [CrossRef]
138. Wu, Y.; Tiri, R.N.E.; Bekmezci, M.; Altuner, E.E.; Aygun, A.; Mei, C.; Yuan, Y.; Xia, C.; Dragoi, E.N.; Sen, F. Synthesis of novel activated carbon-supported trimetallic Pt-Ru-Ni nanoparticles using wood chips as efficient catalysts for the hydrogen generation from $NaBH_4$ and enhanced photodegradation on methylene blue. *Int. J. Hydrogen Energy* **2023**, *48*, 21055–21065. [CrossRef]
139. Kumar, R.; Kumar, K.; Thakur, N.; Umar, A.; Ibrahim, A.A.; Akbar, S.; Baskoutas, S. Green synthesis and multifunctional properties of Cu/NiO nanocomposite using *Commelina benghalensis* leaf extract. *Chemosphere* **2024**, *362*, 142805. [CrossRef]
140. Kareem, M.; Babu, H.; Lakshmi, G.V. *Eco Friendly Synthesis of Cu-Ni Nanocomposite Using Terminalia chebula Extract, Potential Microbial Activity and Catalytic Degradation Studies*; Elsevier: Amsterdam, The Netherlands, 2023. [CrossRef]
141. Alruqi, S.S.; AL-Thabaiti, S.A.; Khan, Z. Iron-nickel bimetallic nanoparticles: Surfactant assisted synthesis and their catalytic activity. *J. Mol. Liq.* **2019**, *282*, 448–455. [CrossRef]
142. Karthick, M.; Surendhiran, S.; Jagan, K.S.G.; Savitha, S.; Vidaarth, T.M.N.; Balu, K.S.; Jaganathan, M.; Karthik, A.; Kalpana, B. Synthesis and characterization of *Araucaria columnaris* leaf-mediated NiO nanoparticles for removal of pharmaceutical pollutants in municipal water bodies. *Appl. Phys. A* **2023**, *129*, 608. [CrossRef]

143. Fardood, S.T.; Moradnia, F.; Aminabhavi, T.M. Green synthesis of novel $Zn_{0.5}NiO_{0.5}FeCrO_4$ spinel magnetic nanoparticles: Photodegradation of 4-nitrophenol and aniline under visible light irradiation. *Environ. Pollut.* **2024**, *358*, 124534. [CrossRef] [PubMed]
144. Honarmand, M.; Naeimi, A.; Rezakhani, M.S.; Chaji, M.A. Ni/NiO doped chitosan-cellulose based on the waste of barley and shrimp for degradation of ciprofloxacin antibiotic. *J. Mater.* **2022**, *18*, 4060–4074. [CrossRef]
145. Fatimah, I.; Citradewi, P.W.; Purwiandono, G.; Hidayat, H.; Sagadevan, S. Nickel oxide decorated reduced graphene oxide synthesized using single bioreactor of *Pometia pinnata* leaves extract as photocatalyst in tetracycline photooxidation and antibacterial agent. *Desalination Water Treat.* **2023**, *298*, 117–126.
146. Jeoffrey, A.C.; Ramalingam, S.J.; Murugaiah, K.; Balu, A.R. One-pot synthesis of rGo-NiO/CdO nanocomposite materials for the photocatalytic degradation of phenol from waste waters and the study of resistance against *Staphylococcus aureus*. *Hybrid Adv.* **2023**, *3*, 100064. [CrossRef]